JGR Oceans

RESEARCH ARTICLE
10.1029/2021JC017787

Drivers of Coral Reconstructed Salinity in the South China Sea and Maritime Continent: The Influence of the 1976 Indo-Pacific Climate Shift

Ankitha Kannad[1], Nathalie F. Goodkin[1,2,3], Dhrubajyoti Samanta[3], Sujata A. Murty[4], Riovie D. Ramos[5], Jason E. Smerdon[6], and Arnold L. Gordon[6]

[1]Earth and Planetary Sciences, American Museum of Natural History, New York City, NY, USA, [2]Asian School of the Environment, Nanyang Technological University, Singapore, Singapore, [3]Earth Observatory of Singapore, Nanyang Technological University, Singapore, Singapore, [4]Atmospheric and Environmental Sciences, University at Albany, Albany, NY, USA, [5]Department of Environmental Science, William Paterson University, Wayne, NJ, USA, [6]Lamont-Doherty Earth Observatory, Columbia University, Palisades, NY, USA

Abstract The flow of Pacific water into the Indian Ocean via the South China Sea (SCS) and Maritime Continent (MC) plays an important role in the ocean thermohaline circulation providing the only low-latitude pathway for the inter-ocean exchange of heat and salt. The transport of the SCS and Indonesian throughflows is modulated by the East Asian monsoon and major climate modes associated with the Pacific and Indian Oceans. As an indicator of surface layer buoyancy, sea surface salinity (SSS) is critical to rates of exchange but instrumental records of SSS are short and sparse. Using empirical orthogonal functions, a synthesis of proxy-based reconstructions of SSS from coral $\delta^{18}O$ is used to study the role of climate variability on long-term SSS behavior in the region. The leading mode of SSS variability in the boreal winter and summer responds to the influence of the 1976 Indo-Pacific climate shift. At multi-decadal timescales, only the East Asian monsoon and the Indian Ocean Dipole (IOD) retain their signal in winter and summer SSS after 1976. At higher frequencies, winter SSS shifts from having a strong East Asian monsoon signal to a more dominant impact of the IOD and the El Niño Southern Oscillation (ENSO) following the shift. In the summer, only a change in ENSO's influence on SSS variability is observed after 1976. The recent intensification and dominance of the IOD and ENSO in driving SSS variability in the SCS and MC may influence circulation in the regional throughflows and perhaps global thermohaline circulation.

Plain Language Summary Southeast Asia, encompassing the South China Sea (SCS) and the Maritime Continent (MC), is the only pathway for the exchange of waters between the tropical Pacific and Indian Oceans. Any modifications made to the temperature and salinity of the waters entering the region are then spread around the Earth through the ocean's thermohaline circulation, an important regulator of global climate. Salinity changes, in particular, are driven by the monsoons and major climate systems in the Indian and Pacific Oceans. A major shift in the state of the region's climate occurred around 1976 but its impact on salinity is poorly understood as instrumental records in this region are short and sparse. Corals document salinity of the surrounding seawater allowing us to extend our records beyond the instrumental period and assess long-term impacts on salinity. Using a synthesis of coral sites from the SCS and the MC, we find that climate systems in the Indian and Pacific Oceans influence regional salinity more frequently after the 1976 climate shift by altering transport of ocean waters in the region. This may have implications for the region's influence on the global thermohaline circulation.

Key Points:

- Multi-decadal salinity variability in the Indonesian and South China Seas have temporally stable relationships to the Indian Ocean Dipole (IOD) and East Asian winter monsoon (EAWM)
- The influence of the IOD and El Niño Southern Oscillation on high-frequency salinity behavior intensifies after the 1976 Indo-Pacific climate shift
- EAWM high-frequency influence on salinity variability decreases following the 1976 climate shift

Supporting Information:

Supporting Information may be found in the online version of this article.

Correspondence to:

A. Kannad,
akannad@ucsd.edu

Citation:

Kannad, A., Goodkin, N. F., Samanta, D., Murty, S. A., Ramos, R. D., Smerdon, J. E., & Gordon, A. L. (2022). Drivers of coral reconstructed salinity in the South China Sea and Maritime Continent: The influence of the 1976 Indo-Pacific climate shift. *Journal of Geophysical Research: Oceans*, *127*, e2021JC017787. https://doi.org/10.1029/2021JC017787

Received 15 JUL 2021
Accepted 17 MAY 2022

Author Contributions:

Conceptualization: Nathalie F. Goodkin, Sujata A. Murty, Arnold L. Gordon
Formal analysis: Ankitha Kannad
Investigation: Ankitha Kannad
Methodology: Ankitha Kannad, Nathalie F. Goodkin, Dhrubajyoti Samanta, Jason E. Smerdon
Project Administration: Nathalie F. Goodkin
Software: Ankitha Kannad

1. Introduction

Seawater transport through the South China Sea (SCS) and the Maritime Continent (MC) is the only tropical pathway for the exchange of water between the Pacific and the Indian Oceans, playing an important role in the global thermohaline circulation (Gordon, 2001). Waters from the Pacific Ocean are significantly freshened and cooled by mixing in the SCS and MC before exiting into the Indian Ocean (Sprintall et al., 2014). These water masses then spread across the Indian Ocean with a component reaching the South Atlantic Ocean through a branch of the Agulhas Current that travels around the southern rim of Africa (Godfrey, 1996; Gordon, 1986). Once in the Atlantic Ocean, these waters are transported northward until they are sufficiently cooled to sink and

Supervision: Nathalie F. Goodkin
Visualization: Ankitha Kannad
Writing – original draft: Ankitha Kannad
Writing – review & editing: Nathalie F. Goodkin, Dhrubajyoti Samanta, Sujata A. Murty, Riovie D. Ramos, Jason E. Smerdon, Arnold L. Gordon

become an important component in the formation of North Atlantic Deep Water (Godfrey, 1996; Gordon, 1986). Variation in water properties or volume transport in the MC and SCS (e.g., Samanta et al., 2021) therefore have important consequences both regionally within the Pacific and Indian Oceans, and globally through the modification of water masses responsible for distributing heat across the planet (Gordon, 1986, 2001).

The South China Sea Throughflow (SCSTF) represents a key component of regional circulation. It is driven by the injection of saline North Pacific Ocean water into the SCS through the Luzon Strait (Figure 1; Qu et al., 2000; Wyrtki, 1961), primarily due to an intrusion of Kuroshio water (Caruso et al., 2006; Centurioni et al., 2004; Liang et al., 2008; Nan et al., 2015; Wyrtki, 1961). The average transport through the Luzon Strait is estimated to be 4.4 Sv annually (Fang et al., 2005). A majority of these SCSTF waters (~3.5 Sv) travel southwards and enter the Indonesian archipelago through the Java Sea (Fang et al., 2005; Qu et al., 2009). In addition to contributions by the SCSTF, Pacific trade winds augment sea surface height along the western tropical Pacific Ocean, creating a pressure gradient that drives the southward flow of tropical Pacific waters through the Indonesian Seas into the Indian Ocean, referred to as the Indonesian throughflow (ITF; Wyrtki, 1987). Approximately 13 Sv of the total 15 Sv of ITF transport moves through the Makassar Strait (Gordon et al., 2010) before being exported into the Indian Ocean mainly through the Lombok Strait (2.6 Sv), Ombai Strait (4.9 Sv), and Timor Passage (7.5 Sv; Figure 1; Sprintall et al., 2009).

Regional climate processes are critical drivers of the SCSTF and ITF. Seasonal variation in transport is dependent on the East Asian monsoons (Masumoto & Yamagata, 1996), which are defined by directional changes of winds in East and Southeast Asia that induce reversing surface ocean circulations. During the boreal winter monsoon, winds from the north-east (Lau & Li, 1984) enhance surface transport through the Luzon Strait and into the SCS (Qu et al., 2000). In the southern Makassar Strait, winter monsoonal winds drive buoyant surface waters from the Java Sea into the Strait (Gordon et al., 2003), inhibiting the flow of warm, saline Pacific surface layer waters into the Indian Ocean (Gordon et al., 2003). The boreal summer monsoon is characterized by strong winds from the south-west over the SCS and MC that dissipate the SCS influence and enhance surface throughflows.

Interannual variability in the Indian and Pacific Oceans also alters surface ocean circulation, as well as evaporation and precipitation patterns across the SCS and MC. In the Pacific Ocean, the dominant interannual mode of climate variability (with a period of 3–7 yr) is the El Niño Southern Oscillation (ENSO) which is characterized by anomalous warming or cooling of the eastern equatorial Pacific Ocean based on the strength of trade winds over the region (Bjerknes, 1969; Sarachik & Cane, 2010). The positive phase of ENSO, referred to as El Niño, strengthens the SCSTF by shifting the North Equatorial Current bifurcation latitude northward, leading to increased westward Luzon Strait transport (Qu et al., 2004). During the El Niño phase, fresher waters from the SCS enter the Sulawesi Sea and inhibit the surface flow of western Pacific Ocean waters into the ITF through the Mindanao Current (Gordon et al., 2012). During La Niña, the negative phase of ENSO, the SCSTF is weaker and the contribution of the Mindanao Current to the ITF is greater. This mechanism allows ENSO to modulate the salinity of the Makassar Strait and consequently the Lombok Strait (Gordon et al., 2010). The Indian Ocean Dipole (IOD), defined as the difference in sea surface temperature (SST) between the western (10°S–10°N, 50°E–70°E) and eastern (10°S–0°N, 90°E–110°E) tropical Indian Ocean (Hameed, 2018; Saji et al., 1999) on interannual timescales (3–5 yr), also interacts with the ITF through its influence on atmospheric circulation over the MC, with enhanced (reduced) convection and precipitation over the eastern Indian Ocean and western Pacific during negative (positive) phases of the IOD (R. Wu & Kirtman, 2004). Kelvin waves from the equatorial Indian Ocean also propagate IOD impacts into the Indonesian Seas (Sprintall et al., 2009). There are other modes of climate variability in the Indian Ocean but only the IOD has been found to have a strong influence on the ITF and SCSTF (Sprintall et al., 2009).

Decadal variability (20–30 yr) is influenced by the Interdecadal Pacific Oscillation (IPO), defined as a tripole pattern in SST over the Pacific Ocean (Power et al., 1999). The IPO is a larger-scale pattern than the Pacific decadal oscillation (PDO) which only evaluates the northern Pacific (Henley et al., 2015; Power et al., 1999). Through its modulation of ocean temperature, the IPO also influences the phases of the ENSO (Dong et al., 2018; Power et al., 1999), the IOD (Jin et al., 2018; Ummenhofer et al., 2020) and the monsoons (Kim et al., 2014).

Previous studies have also identified an unprecedented shift in the state of the Indo-Pacific climate around 1976 (Trenberth & Hoar, 1996). The 1976 climate shift was characterized by a sharp increase in the large-scale warming of the central and eastern tropical Pacific and an eastward shift of convective activity over the tropical

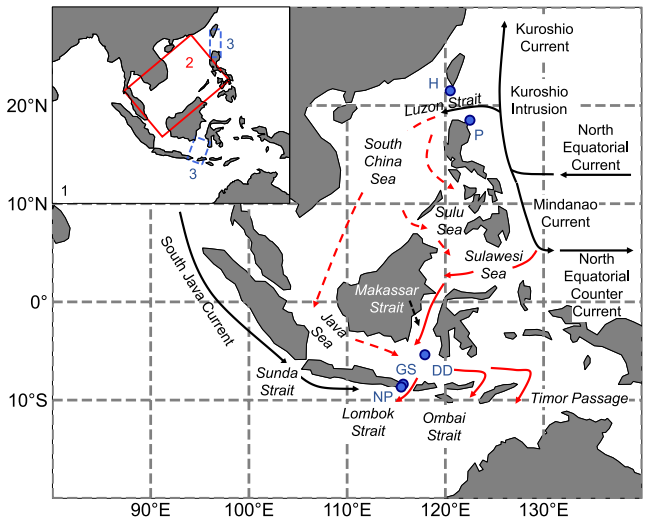

Figure 1. Circulation of surface waters through the Maritime Continent (solid red arrows) and the South China Sea (dashed red arrows) drawn from Pacific western boundary and Indian eastern boundary currents (solid black arrow). Coral sites are shown with blue dots and labeled as: H = Houbihu, P = Palaui, DD = Doangdoangan Besar, GS = Gili Selang, and NP = Nusa Penida. Inset describes the regions analyzed in greater detail: (1) the whole region, (2) the South China Sea (solid red box), and (3) the Luzon, Lombok, and southern Makassar Straits that encompass the coral sites examined (dashed blue boxes).

western Pacific (Graham, 1994). The period was also coincident with an increase in the frequency of ENSO events (Trenberth, 1990) and a shift to a positive phase of the IPO (Meehl et al., 2009). By modifying the strength of easterlies, the 1976 climate shift is also found to have impacted surface circulation in the MC (Murty et al., 2017; Wainwright et al., 2008) and SCS (Liu et al., 2010) that altered regional salinity and temperature (Murty et al., 2017). However, whether this was a result of natural climate variability or anthropogenic climate change is still not well understood (Graham, 1994; Meehl et al., 2009; Trenberth & Hoar, 1996; Wang et al., 2019).

Salinity provides a useful means of examining the climate drivers of the SCSTF and the ITF. Nan et al. (2016) attributed a freshening of the SCS in the early 1990s to a shift to the cool phase of the PDO (Mantua et al., 1997; Newman et al., 2016), leading to a weakening of the Kuroshio Intrusion. Model results of ITF transport also showcase a reduction or even reversal of the throughflow when salinity effects on transport are neglected (Murtugudde & Busalacchi, 1998).

Studying the climate drivers of the SCSTF and the ITF using salinity is challenging because observational salinity data in the SCS and MC is limited. In situ observations in the region, including bathythermograph networks (Ishii & Kimoto, 2009; Meyers et al., 1995) and mooring arrays like ARLINDO (Susanto & Gordon, 2005) and INSTANT (Sprintall et al., 2004), were only initiated in the 1980s. Reanalysis products like Simple Ocean Data Assimilation (SODA) that assimilate observations with an ocean circulation model are also known to be unreliable prior to the 1980s due to limited historical SSS records (Carton et al., 2000). Proxy-climate records thus provide an opportunity to characterize the climate drivers of the throughflow over timescales that cannot be studied by instrumental records alone. Among the available proxy-climate records, corals provide a unique paleo-archive of salinity as they are stationary throughout their life and their growth patterns allow for sub-annual resolution sampling that yields seasonal reconstructions of temperature and salinity (Grottoli & Eakin, 2007). The coral-based salinity proxy relies on changes in the skeletal oxygen isotope composition ($\delta^{18}O$) which is a function of temperature and salinity (Dunbar & Wellington, 1981; Epstein et al., 1953). Independent gridded temperature records or temperature-only proxy reconstructions can thus be employed to isolate $\delta^{18}O$ changes driven only by salinity, termed $\delta^{18}O$ of seawater ($\delta^{18}O_{sw}$; McCulloch et al., 1994).

Several salinity reconstructions exist for the MC and SCS (Murty et al., 2017, 2018; Ramos, Goodkin, Druffel, Fan, & Siringan, 2019; Ramos et al., 2020, 2017; Ramos, Goodkin, Siringan, & Hughen, 2019). Each site identifies different local drivers of salinity consistent with our knowledge of the major climate drivers in the MC and SCS regions. Despite the availability of these multiple records, no study has linked them together to understand the covariance of salinity across the region. We, therefore, perform a multi-site synthesis using empirical orthogonal functions (EOFs) to characterize coral records along the SCSTF and ITF to investigate (a) their ability to capture regional variability in salinity, (b) the climate drivers influencing them, and (c) the impact of the 1976 Indo-Pacific climate shift on the region.

2. Data and Methods

2.1. Coral Records

2.1.1. Identification of Coral Records

Published coral-based salinity records located in the SCS and MC were identified for analysis based on the following criteria: (a) their $\delta^{18}O$ coral data was publicly available, (b) the data had a sub-seasonal resolution, and (c) the $\delta^{18}O$ records were converted to sea surface salinity (SSS) to ensure that only data capturing a salinity signal are examined. Five coral records met the selection criteria (Murty et al., 2017, 2018; Ramos, Goodkin, Druffel, et al., 2019; Ramos et al., 2020, 2017; Ramos, Goodkin, Siringan, et al., 2019); the coral locations are shown in Figure 1 and additional information on the records are given in Table 1. Calibrations and validity of the

Table 1
Information on Salinity Data and Climate Indices Used in the Analysis Including Description, Months Used in the Comparison, Location, and Reference of the Data Source

	Data	Seasons	Location	Reference
Coral records SSS	Doangdoangan Besar (DD), Indonesia	JFM JAS	5.382°S, 117.914°E	Murty et al. (2017)
	Gili Selang (GS), Indonesia		8.38°S, 115.71°E	Murty et al. (2018)
	Nusa Penida (NP), Indonesia		8.67°S, 115.51°E	Murty et al. (2018)
	Palaui (P), Philippines	DJFM JJAS	18.5°N, 122.2°E	Ramos, Goodkin, Druffel, et al. (2019) and Ramos, Goodkin, Siringan, et al. (2019)
	Houbihu (H), Taiwan		21.9°N, 120.7°E	Ramos et al. (2020)
SODA SSS	Region	JFM JAS	20°S–30°N, 80°E−140°E	Carton and Giese (2008)
	South China Sea (SCS)		3°S–12°N, 108°E−130°E	
	Straits		10°S–6°S, 118°E−124°E; 17°N–24°N, 120°E−122.7°E	
Climate indices	EAWM	DJF	110°E−160°E, 40°N–65°N	D'Arrigo et al. (2005)
	ENSO	Annual	5°S–5°N, 120°W–170°W	Trenberth (1997)
	IPO		25°N–45°N, 140°E−145°E; 10°S–10°N, 170°E−90°W; 50°S–15°S, 150°E−160°W	Henley et al. (2015)
	IOD	SON (−1)	10°S–10°N, 50°E−70°E; 10°S–0°N, 90°E−110°E	Saji et al. (1999)

previously published salinity records can be found in Supporting Information (Figure S2 in Supporting Information S1). An additional record (Cahyarini et al., 2014) only reported a reconstructed SSS anomaly and the record only extends till 2003. The δ^{18}O anomaly does not correlate well to SSS with a reported r of 0.50 (Cahyarini et al., 2014) and no significant correlation to the salinity products used in this study (Figure S2f in Supporting Information S1). There were other δ^{18}O records from this region, but they either did not reconstruct salinity from their proxy data (Abram et al., 2008; Charles et al., 2003; Krawczyk et al., 2020; Linsley et al., 2017) or did not observe a salinity signal (Abram et al., 2015).

The coral records used in this study are located at major channels of inflow and outflow for the SCSTF and ITF (Figure 1). Two sites, Houbihu and Palaui, encompass the northern and southern edges of the Luzon Strait (Ramos, Goodkin, Druffel, et al., 2019; Ramos et al., 2020, 2017; Ramos, Goodkin, Siringan, et al., 2019). Advected waters from the SCS into the Makassar Strait are recorded by the Doangdoangan Besar coral (Murty et al., 2017). Gili Selang and Nusa Penida on either end of the Lombok Strait represent the outflow of the ITF into the Indian Ocean (Murty et al., 2018).

For the selected coral records, the salinity signal within δ^{18}O was larger than that of temperature and each record was quantitatively converted to salinity based on calibration to the reanalysis product SODA (v.2.2.4 with 0.5° × 0.5° grid at depth 5 m, Carton & Giese, 2008). Except for Doangdoangan Besar, these coral records reconstruct salinity from δ^{18}O directly. The Doangdoangan Besar record is δ^{18}O of seawater derived by removing the SST signal from the coral δ^{18}O record (Murty et al., 2017). SST is obtained from the reanalysis product Hadley Center for Sea Ice and Sea Surface Temperature reanalysis product (HadISST, 0.5° × 0.5° grid, Rayner et al., 2003). At Doangdoangan Besar, SST was estimated to only describe 29%–39% of the coral δ^{18}O variability. Reconstructed salinity at each site ranges from approximately 31–38 psu.

2.1.2. Standardization of Coral Records

To ensure the compatibility and consistency of the coral SSS records in subsequent analysis, they were: (a) examined over the shared period of overlap (1930–2010), (b) re-sampled at a bimonthly resolution to match records from Doangdoangan Besar, Gili Selang and Nusa Penida, (c) averaged over the boreal winter and summer to identify seasonal climate drivers, (d) linearly detrended, and (e) normalized to unit variance and centered to zero mean by dividing each record with its standard deviation and subtracting the mean from each record, both of which were determined over the 1930–2010 interval.

The corals used in this study were sampled at different time resolutions and therefore, interpolated either to monthly or bi-monthly resolution. For the higher resolution corals, only points in time corresponding to the lower resolution samples were averaged to generate seasonal records.

The seasons used in the averaging of the coral records are based on their published analyses and summarized in Table 1. Doangdoangan Besar, Gili Selang, and Nusa Penida reconstruct salinity for the boreal winter (January–March, JFM) and boreal summer (July–September, JAS). These also correspond to the respective dry and wet seasons in the southern Indonesian archipelago (Murty et al., 2017, 2018). The seasons for Palaui (Ramos, Goodkin, Druffel, et al., 2019; Ramos, Goodkin, Siringan, et al., 2019) and Houbihu (Ramos et al., 2020) similarly correspond to boreal winter and summer but they average slightly longer periods, December–March (DJFM) and June–September (JJAS) respectively.

2.1.3. EOFs of Coral Records

EOF analysis was employed on the standardized coral records to identify dominant patterns in the reconstructed salinity. Using singular value decomposition, the principal components (PCs), the variance described by them and their corresponding spatial variability (EOFs) were derived from the decomposed matrix of the coral records (Thomson & Emery, 2014; Zhang & Moore, 2015).

The Overland and Preisendorfer (1981) method was used to evaluate EOF statistical significance. In this process, EOF analysis was performed on red noise that had the same resolution, period, sample size, and normalization as the original data. The randomized data set was sampled from a normal distribution to remain consistent with a majority of the coral records. EOF analysis was performed on 500 iterations of these red noise realizations to determine the 95% confidence level of this ensemble. To compare the red noise and coral EOFs, eigenvalues of both calculations were normalized by dividing by their sum. If the normalized eigenvalues of the coral records were greater than the 95% confidence level, the variability they describe was taken to be distinguishable from red noise and hence, significant.

2.2. Reanalysis Salinity Record

2.2.1. EOFs of Instrumental Salinity

The reanalysis product SODA v.2.2.4 (Carton & Giese, 2008) was used to evaluate the geographical scope of the coral EOFs. SODA v.2.2.4 assimilates observational ocean data with an ocean circulation model, based on the Geophysical Fluids Dynamics Laboratory Modular Ocean Model, to develop an estimate of ocean state from 1871 to 2010 (Carton & Giese, 2008; Giese & Ray, 2011). The reanalysis product is shown to be a reasonable approximation of transport in the ITF and SCS throughflow in modern times (e.g Du & Qu, 2010; Linsley et al., 2017; Tillinger & Gordon, 2009). Before the 1980s, however, the SODA data set is not as accurate because historical records, particularly of SSS, were limited and unreliable (Carton et al., 2000). Despite this limitation, previous studies have used SODA to examine seasonal and lower frequency trends in the Indo-Pacific region (Du & Qu, 2010; England & Huang, 2005; Schoenefeldt & Schott, 2006) suggesting its continued reliability at the timescales relevant for this study. Several other reanalysis products, such as EN4 (Good et al., 2013), have also been used to examine long-term variability in the Indo-Pacific with similar results (e.g., Chakravorty et al., 2014). The SODA SSS product is used herein because it is already well correlated with the examined coral records over their calibration period (Figure S2 in Supporting Information S1; Murty et al., 2017, 2018; Ramos, Goodkin, Druffel, et al., 2019; Ramos et al., 2020, 2017; Ramos, Goodkin, Siringan, et al., 2019).

Three spatial domains of the gridded SODA salinity were explored as shown in Figure 1. The entire region (Figure 1, inset box 1) encompassed the SCS, MC, and passageways of the Indian and Pacific Ocean (20°S–30°N, 80°E−140°E, and 5 m depth). Two additional subregions are the SCS (Figure 1, inset box 2) and the Straits where the coral sites were located (Figure 1, inset box 3). All three were compared to the coral EOFs to further identify regional influences. SODA SSS EOFs for the same boreal summer (JAS) and winter (JFM; Table 1) were evaluated for significance against red noise as previously described.

2.3. Climate Indices

Climate indices were employed to investigate tropical climate variability influencing the EOFs of reconstructed salinity. Published indices were used to examine climate variability with widely accepted definitions of the climate modes.

The East Asian winter monsoon (EAWM) index records the strength of the winter monsoon winds for the months December–February (DJF; Table 1). D'Arrigo et al. (2005) compute the index by summing zonal sea level pressure differences between 110°E and 160°E over the latitude band 40°N–65°N using the formula from B. Wu and Wang (2002) and Hadley Center's GMSLPv2.1f data set (Basnett & Parker, 1997).

The ENSO and IPO indices describe dominant modes of climate variability that originate in the Pacific Ocean. The employed ENSO index (Niño3.4; Trenberth, 1997) is defined as the average SST anomaly across the equatorial Pacific (5°S–5°N, 120°W–170°W) calculated using HadISST (Rayner et al., 2003; retrieved from https://climatedataguide.ucar.edu/climate-data/nino-sst-indices-nino-12-3-34-4-oni-and-tni). The employed IPO index is the difference between SST anomalies averaged over the eastern equatorial Pacific (10°S–10°N, 170°E−90°W) and SST anomalies averaged over the central North Pacific (25°N–45°N, 140°E−145°E), and central South Pacific (50°S–15°S, 150°E−160°W; Henley et al., 2015). SST is derived from the HadISSTv2.1.0.0 data set (Titchner & Rayner, 2014). Both the ENSO and IPO indices are annually averaged because they are both active throughout the year (Table 1).

The Dipole Mode Index represents the IOD, the only mode of tropical climate variability originating in the Indian Ocean (Saji et al., 1999). It has the largest signal from September to November (SON) and is averaged accordingly (Table 1). The published index is the difference between SST anomalies in the western (10°S–10°N, 50°E−70°E) and eastern (10°S–0°N, 90°E−110°E) Indian Ocean. SST anomalies are derived from the GISSTv2.3b data set (Rayner et al., 1996).

2.4. Comparing PCs of Coral Records to Gridded Salinity and Climate Indices

Cross-coherence analysis using a multitaper method with adaptive weighting and bias correction was employed to compare the coral and SODA SSS PCs (Huybers & Denton, 2008). Coherence was estimated using eight windows and phase uncertainty was determined with 100 Monte Carlo simulations. Frequencies with coherence greater than the 95% confidence level indicate timescales at which the coral PCs best represent the PCs of regional salinity (Figure 1 inset box 1). To evaluate potential sources of the SSS regional variability, cross-coherence analysis was also used to compare the coral SSS PCs with the PCs of the subregions (SCS and Straits) shown in Figure 1 inset boxes 2 and 3 respectively.

Once time bands of significant coherence between the coral and regional SODA PCs were identified, these frequencies were used to investigate climate drivers of regional salinity. Time bands with a minimum length of 1 yr were chosen to match the sampling frequency of the seasonal coral records. The coral PCs and climate indices were filtered for these frequencies using a bandpass filter with a Hamming window of order 25.

To investigate their time-varying coherence and phase, the climate indices were also independently compared to coral SSS PCs at all frequencies using wavelet coherence (Grinsted et al., 2004). The 95% confidence level was calculated against red noise using 300 Monte Carlo simulations. Additionally, the wavelet coherence of coral and regional SODA SSS PCs (domain shown in Figure 1 inset box 1) were used to evaluate the regional significance of this analysis.

3. Results and Discussion

3.1. Comparing EOFs of Reconstructed and Regional Salinity

EOF analysis of the extended coral SSS records yields significant EOF1s for the winter and summer that explain 34% and 36% of the variance in the data, respectively (Figures 2a and 2c and Figures S1a and S1e in Supporting Information S1). Except for Nusa Penida at the southern end of the Lombok Strait, the remaining coral sites are relatively equally weighted for both the summer and winter EOF1 (Figures 2a and 2c). Houbihu is out of phase with Gili Selang and Doangdoangan Besar for both seasons while Palaui shifts from behaving like Doangdoangan Besar and Gili Selang in the winter to being similar to Houbihu in the summer.

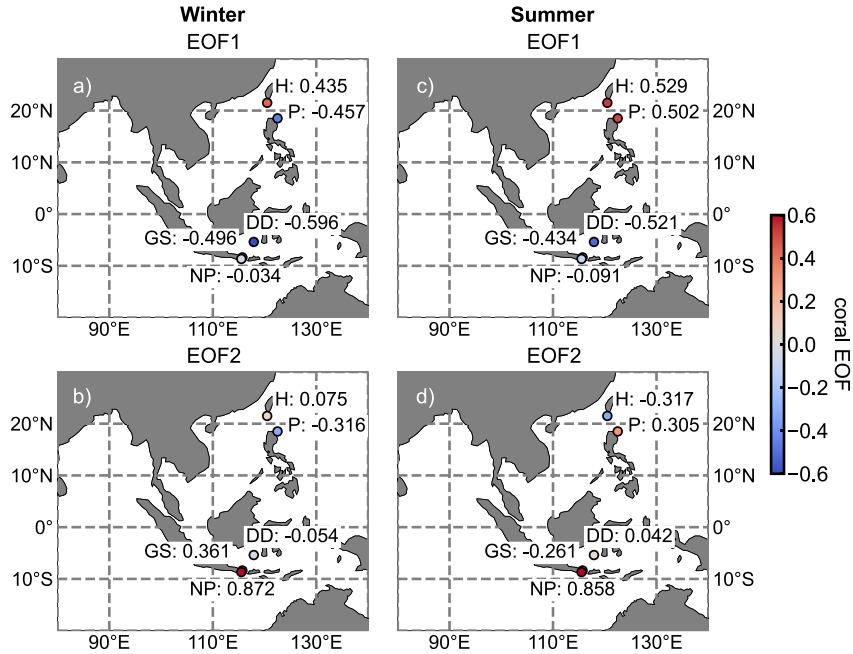

Figure 2. Spatial variability in coral reconstructed salinity: (a) winter EOF1, (b) winter EOF2, (c) summer EOF1, and (d) summer EOF2. Coral sites are labeled as: H = Houbihu, P = Palaui, DD = Doangdoangan Besar, GS = Gili Selang, and NP = Nusa Penida. The magnitude and sign of the colorbar represents the weighting of each coral site on the EOF. For both seasons, coral EOF1 is approximately equally weighted in magnitude by all the sites except the southernmost NP. A dipole-like behavior is observed between the site closest to the Pacific Ocean (H) and the more interior sites (DD and GS) with P showing greater seasonal variation. NP contributes much of the variability of coral EOF2 for both seasons.

For both seasons, EOF1 of coral SSS indicates that the Luzon Strait (Houbihu), which is closest to the Pacific Ocean, is out of phase with the more interior sites in the MC (Doangdoangan Besar and Gili Selang). Ramos, Goodkin, Druffel, et al. (2019) found that flow through Houbihu is dependent on monsoonal winds that drive advection across the Luzon Strait. When the EAWM is strong, the monsoonal winds increase advection of saline waters from the Pacific Ocean into the Luzon Strait at Houbihu, while also strengthening the circulation from Palaui to the throughflow. The interior sites thus have similar variability in the winter EOF1 when circulation from Palaui to the throughflow is stronger. Without the influence of the EAWM, Houbihu and Palaui variability are more closely related in the summer EOF1 and have distinctly different variability than the interior sites.

While not significant relative to red noise, the second EOF for both seasons records a strong contribution from Nusa Penida relative to the other sites examined (Figures 2b and 2d) and relative to EOF1. Nusa Penida is located at the confluence of the Indian Ocean and ITF. Hence, it provides an opportunity to examine climate processes at a region of export from the MC. Winter EOF2 explains 22% of the variance in the data while summer EOF2 explains 23%. Murty et al. (2018) previously found that winter SSS in Nusa Penida differs from the upstream ITF sites especially during positive phases of the EAWM and suggested Indian Ocean waters may advect northwards into the Lombok Strait during these periods. This monsoon-driven transport is also modulated by ENSO with a reversal of this northward flow observed during El Niño years (Susanto et al., 2007). The climate drivers of Nusa Penida were not previously examined for the summer but flow within the Lombok Strait is known to be southward into the Indian Ocean, influenced by the southeastern monsoonal winds (Susanto et al., 2007). Given the physical significance of the Lombok Strait and Nusa Penida on SSS in the region, we examine the relationship between EOF2 and important climate drivers in the region.

EOFs of the SODA reanalysis product over the domains defined (Figure 1) also return at least 3 significant EOFs (Figures S1b–S1d and S1f–S1h in Supporting Information S1). The domains of the EOFs are shown in Figure 1, and include regional (inset box 1), SCS (inset box 2), and the Straits (inset box 3). To compare EOFs of SODA and reconstructed salinity, only the first two EOFs for each domain are analyzed. Regional SSS EOFs for both seasons describe less variability (~30%–35%) compared to the SCS and Straits boxes (~60%–70%) that likely capture more localized and hence, more covarying changes in salinity.

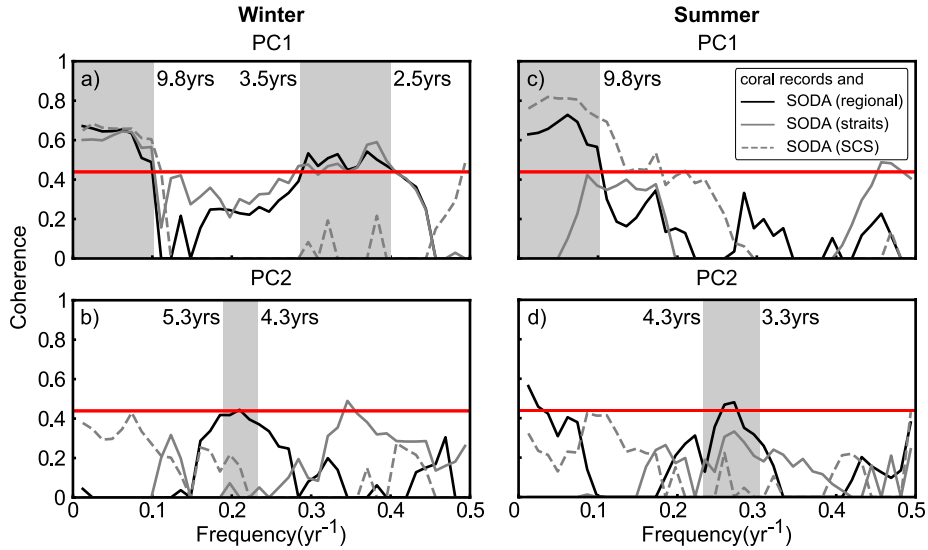

Figure 3. Cross-coherence spectral analysis of significant coral record PCs to corresponding PCs of SODA salinity for boreal winter (a) PC1 and (b) PC2, and boreal summer (c) PC1 and (d) PC2. Frequency bands with coherence greater than the 95% confidence level (red solid line) are shaded gray. For both seasons, coral PC1 is coherent with multidecadal variability in regional SODA salinity while coral PC2 represents interannual variability. Winter coral PC1 is additionally coherent with regional salinity at interannual frequencies.

3.2. Comparing PCs of Reconstructed and Regional Salinity

To determine how well the significant modes of temporal coral SSS variability reflect regional salinity, coral PCs were cross-correlated to the corresponding PCs of SODA SSS across all frequencies and spatial domains (Figure 3). Significant coherence between the coral winter PC1 is found at time scales of <0.1 cycles per year or >9.8 yr per cycle for the regional, SCS and Strait domains (Figure 3a). Hence, at largely decadal periods, the variability of the winter coral PC1 is representative of regional variability across a range of geographical sizes. PC1 is also coherent with regional and Strait salinity over an interannual range of frequencies (2.5–3.5 yr per cycle) but not SCS salinity. Hence, PC1 at these frequencies may describe either ITF or Pacific and Indian Ocean processes that influence the Straits but are not along the main pathway of the SCSTF.

Summer coral PC1 is coherent across the same decadal bands with both the regional and SCS domains but not the Straits (Figure 3c), which is surprising given the approximately equal weighting of the coral sites except Nusa Penida on the PC (Figures 2a and 2c). The PCs of the regional and SCS domains may capture similar salinity variability due to advection of fresher SSS Indonesian waters into the Java Sea and subsequently SCS by the summer southerly monsoon winds (Gordon et al., 2003). Reconstructed and SODA SSS variability in the domain of the Straits may be more influenced by local salinity changes suggesting disconnects between the corals and gridded data.

For winter and summer coral PC2, a short band of coherence is found over an interannual frequency band (4.3–5.3 yr and 3.3–4.3 yr respectively) with the regional SODA PC2 (Figures 3b and 3d). Combined with a lack of correlation to the EOFs of either the SCS or Straits, these results indicate that the second PC may be describing processes originating in the Pacific or Indian oceans rather than internal to the SCS and MC.

3.3. Winter Coral PCs of Reconstructed SSS at Frequencies Related to Regional SSS

At frequencies <8 yr per cycle, the IPO, ENSO, and IOD indices have a more consistent relationship with winter PC1 of reconstructed SSS after 1976. Wavelet analysis that describes the time-varying coherence between these climate indices and winter PC1 indicates a shift from brief periods of high-frequency (<4 yr) coherence to consistent interannual (3–8 yr) coherence after 1976 (Figures 4e–4g). A Hamming window band-pass filter (2.5–3.5 yr) is also applied to winter PC1 and climate indices to evaluate regional processes (Figures 3a and 4). The filtered record is only in phase with the IPO, ENSO, and IOD indices between 1976 and 1995 (Figures 4i–4k). The

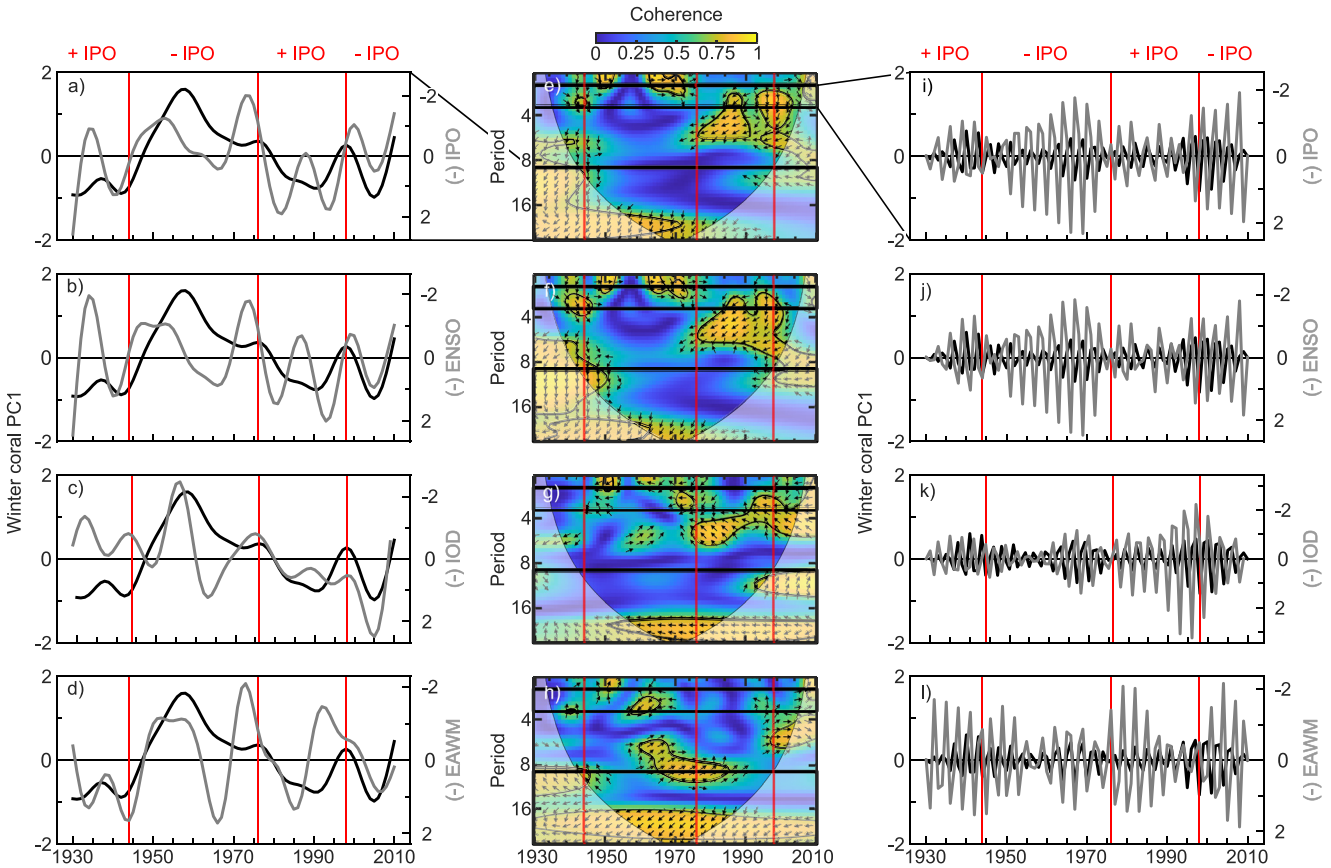

Figure 4. Comparison of winter coral sea surface salinity (SSS) PC1 and climate indices. Low-pass filtered (>9.8 yr) winter PC1 (black solid line) with similarly filtered climate indices (gray solid line) of (a) IPO, (b) ENSO, (c) IOD, and (d) EAWM highlight SSS and climate variability at frequencies describing regional processes. Similarly, winter PC1 (black solid line) at interannual frequencies (2.5–3.5 yr) is compared to filtered (i) IPO, (j) ENSO, (k) IOD, and (l) EAWM (all gray solid line). The axes for the climate indices are inverted. Time-varying coherence is examined using wavelet analyses of coral winter PC1 and (e) IPO, (f) ENSO, (g) IOD, and (h) EAWM. The filtered frequencies in panels (a–d and i–l), which represent regional variability, are indicated with black boxes in panels (e–h). Contours (black) in panels (e–h) indicate the 95% confidence level determined against the red noise null hypothesis and arrows denote the relative phase relationships. The cone of influence is shown in a lighter shade. For both methods of comparison, the important phase shifts of the IPO in 1944, 1976, and 1998 (England et al., 2014) and the 1976 Indo-Pacific climatic shift are marked with red vertical lines.

record also matches the amplitude changes of the IPO and ENSO indices during this period. The EAWM does not exhibit a similar change with winter PC1 after 1976 but instead has scattered coherence at frequencies <14 yr per cycle within the cone of influence (1944–2005; Figure 4h). The filtered interannual PC record (2.5–3.5 yr) has phase but no magnitude agreement with the EAWM index for most of this period from 1955 to 1995 (Figure 4i).

At frequencies >16 yr per cycle, wavelet coherence of winter PC1 is observed with the EAWM and IOD index across the period examined (Figures 4g and 4h) while the IPO and ENSO indices are only coherent with winter PC1 until 1976 (Figures 4e and 4f) when restricted to the cone of influence period (1950–1985). Winter PC1 and climate indices are additionally filtered with a Hamming low-pass filter (>9.8 yr) to examine regional variability. Shifts in winter PC1 between positive and negative regimes also respond to phase shifts of the IPO and ENSO indices (Figures 4a and 4b) with both indices entering a negative mode after 1944 and a positive mode after 1976 (England et al., 2014). A similar pattern is not observed with the IOD and EAWM indices despite their strong wavelet coherence with winter PC1. For the multidecadal IOD index and winter coral PC1 (>9.8 yr), a long-term phase shift of PC1 is observed around 1976 and is coincident with a shift from a predominantly negative to positive IOD (Figure 4c). The EAWM index filtered over the same low frequencies (>9.8 yr) only captures winter coral SSS variability until 1950 and after 1998 (Figure 4d).

In examining the winter coral PC2, all records were bandpass filtered to 4.3–5.3 yr per cycle, where the coral SSS PC reflects regional salinities (Figure 3b). The phase shifts of the IPO have a dominant influence on winter

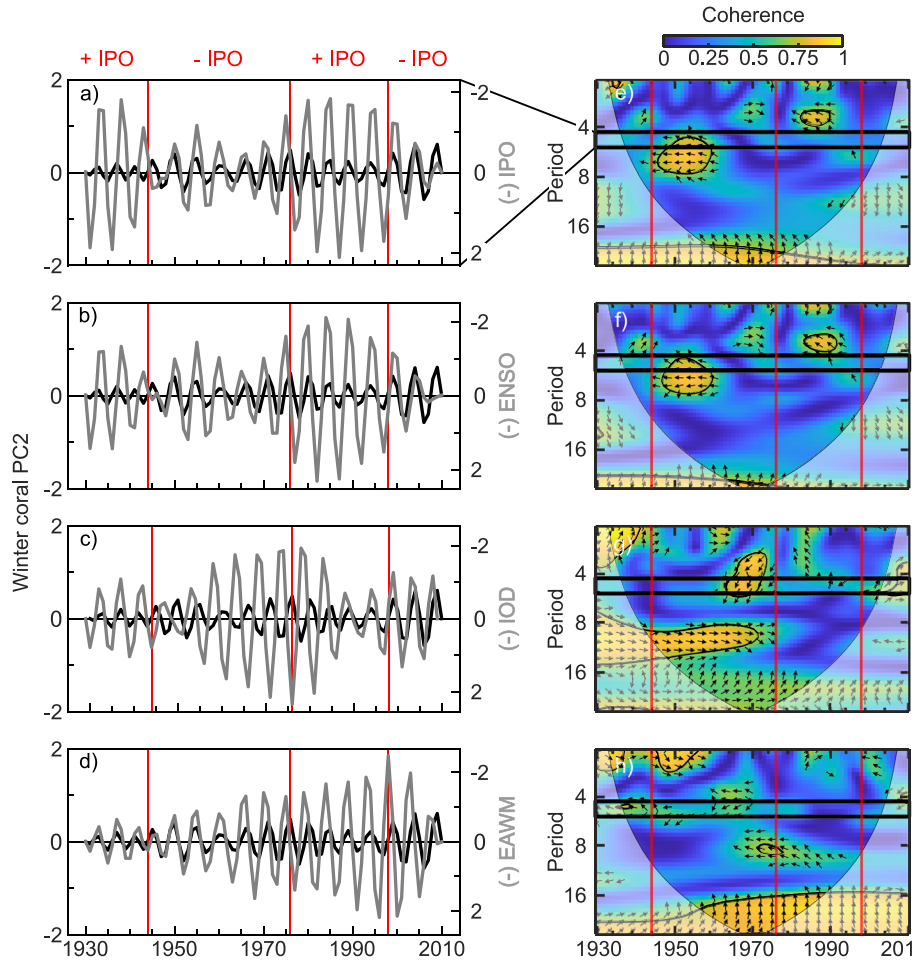

Figure 5. Comparison of winter coral sea surface salinity (SSS) PC2 and climate indices. Band-pass filtered (4.3–5.3 yr) winter PC2 (black solid line) with similarly filtered climate indices (gray solid line) of (a) IPO, (b) ENSO, (c) IOD, and (d) EAWM highlight SSS and climate variability at frequencies describing regional processes. The axes for the climate indices are inverted. Time-varying coherence is examined using wavelet analyses of coral winter PC2 and (e) IPO, (f) ENSO, (g) IOD, and (h) EAWM. The filtered frequencies in panels (a–d) are indicated with black boxes in panels (e–h). Contours (black) in panels (e–h) indicate the 95% confidence level determined against the red noise null hypothesis and arrows describe relative phase relationships. The cone of influence is shown in a lighter shade. For both methods of comparison, the important phase shifts of the IPO in 1944, 1976, and 1998 (England et al., 2014) and the 1976 Indo-Pacific climatic shift are marked with red vertical lines.

PC2 over this interannual band. During the negative modes of the IPO (1944–1976 and 1995–2010; England et al., 2014), the filtered IPO and ENSO indices negatively covary with winter PC2 but match the amplitude changes of the record (Figures 5a and 5b). The indices are similarly out of phase with winter PC2 during positive modes of the IPO (1976–1995; England et al., 2014) but no longer capture the magnitude of this variability (Figures 5a and 5b). Outside of the interannual band, wavelet coherence of the IOD index with winter PC2 occurs over frequencies of 8–16 yr during the negative mode of the IPO from 1944 to 1976 (Figure 5g). The EAWM does not appear to depend on the IPO and is coherent with winter PC2 at low frequencies (>16 yr) across all IPO modes that fall within the cone of influence (Figure 5h).

3.4. Summer Coral PCs of Reconstructed SSS at Frequencies Related to Regional SSS

Similar to the winter coral PC1, the IOD and EAWM index retain their low-frequency influence (>16 yr per cycle) on summer PC1 of reconstructed SSS (Figures 6g and 6h) even after 1976, while the ENSO and IPO indices shift from coherence at lower frequencies (>16 yr per cycle) to higher frequencies (8–12 yr) following the climate shift (Figures 6e and 6f). A lowpass filter (>9.8 yr) is also applied to both the summer coral PC1 and the climate

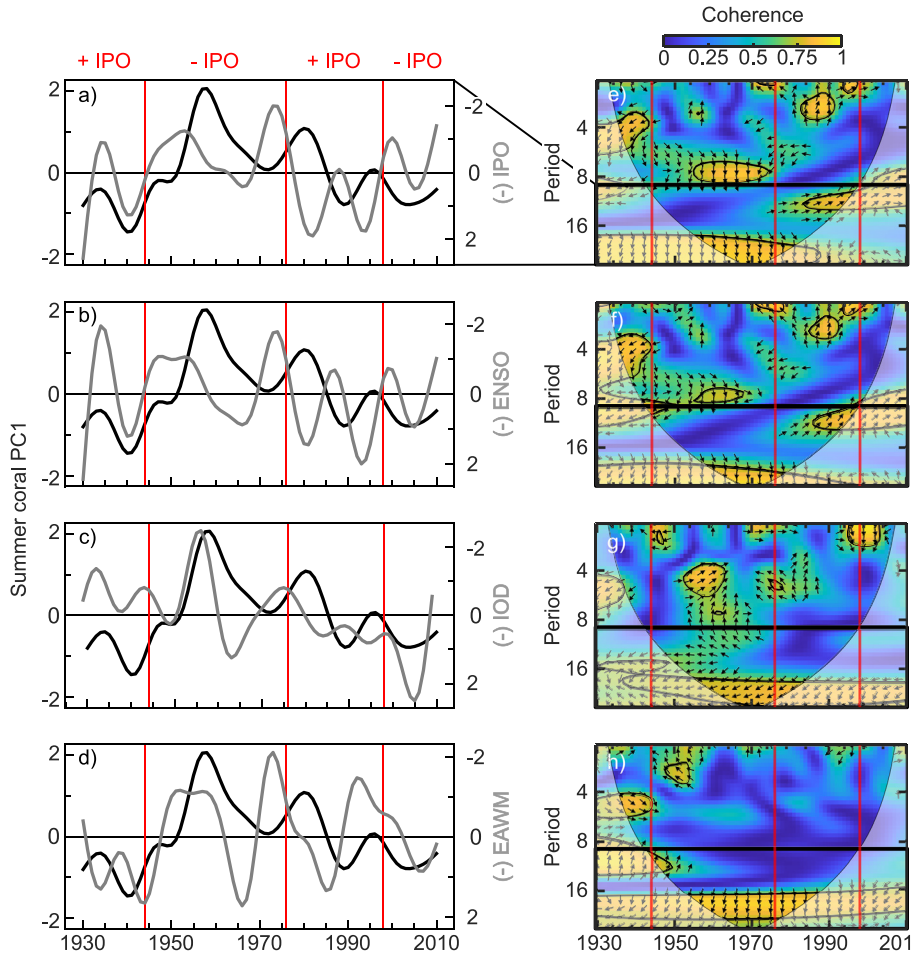

Figure 6. Comparison of summer coral sea surface salinity (SSS) PC1 and climate indices. Low-pass filtered (>9.8 yr) summer PC1 (black solid line) with similarly filtered climate indices (gray solid line) of (a) IPO, (b) ENSO, (c) IOD, and (d) EAWM highlight SSS and climate variability at frequencies describing regional processes. The axes for the climate indices are inverted. Time-varying coherence is examined using wavelet analyses of coral summer PC1 and (e) IPO, (f) ENSO, (g) IOD, and (h) EAWM. The filtered frequencies in panels (a–d) are indicated with black boxes in panels (e–h). Contours (black) in panels (e–h) indicate the 95% confidence level determined against the red noise null hypothesis and arrows describe relative phase relationships. The cone of influence is shown in a lighter shade. For both methods of comparison, the important phase shifts of the IPO in 1944, 1976, and 1998 (England et al., 2014) and the 1976 Indo-Pacific climatic shift are marked with red vertical lines.

indices to evaluate frequencies at which summer PC1 reflects regional variability (Figure 3c; Figure 6). Similar to the winter coral PC1, major phase shifts between positive and negative regimes in the summer PC1 coincide with phase shifts in the IPO and ENSO indices in 1944 and 1976 (England et al., 2014; Figures 6a and 6b). The indices lead changes in summer PC1 by approximately 10 yr (Figures 6a and 6b). A phase shift of the decadal IOD index (>9.8 yr) around 1976 also matches a phase shift in the summer coral in PC1 that occurs approximately 10 yr later in 1985 (Figure 6c). The filtered EAWM index does not capture amplitude changes in summer coral PC1 except for a brief period between 1930 and 1948 when the EAWM is in a predominantly positive mode (Figure 6d).

A pattern similar to the summer coral PC1 is observed when examining the wavelet coherence of summer coral PC2 with the climate indices (Figure 7). The IOD and EAWM index are coherent with summer PC2 at low frequencies (>16 yr) within the cone of influence (Figures 7g and 7h). The ENSO index shifts from lower (>16 yr) to higher (8–16 yr) frequency coherence after 1976, while the IPO is only coherent with summer PC2 (8–16 yr) following the shift (Figures 7e and 7f). A bandpass filter of 3.3–4.3 yr is applied to the summer PC2 and climate indices to reflect frequencies when the coral represents regional salinity (Figure 3d). Almost no wavelet coherence of summer PC2 with the climate indices is observed over this frequency band (Figures 7e–7h). The

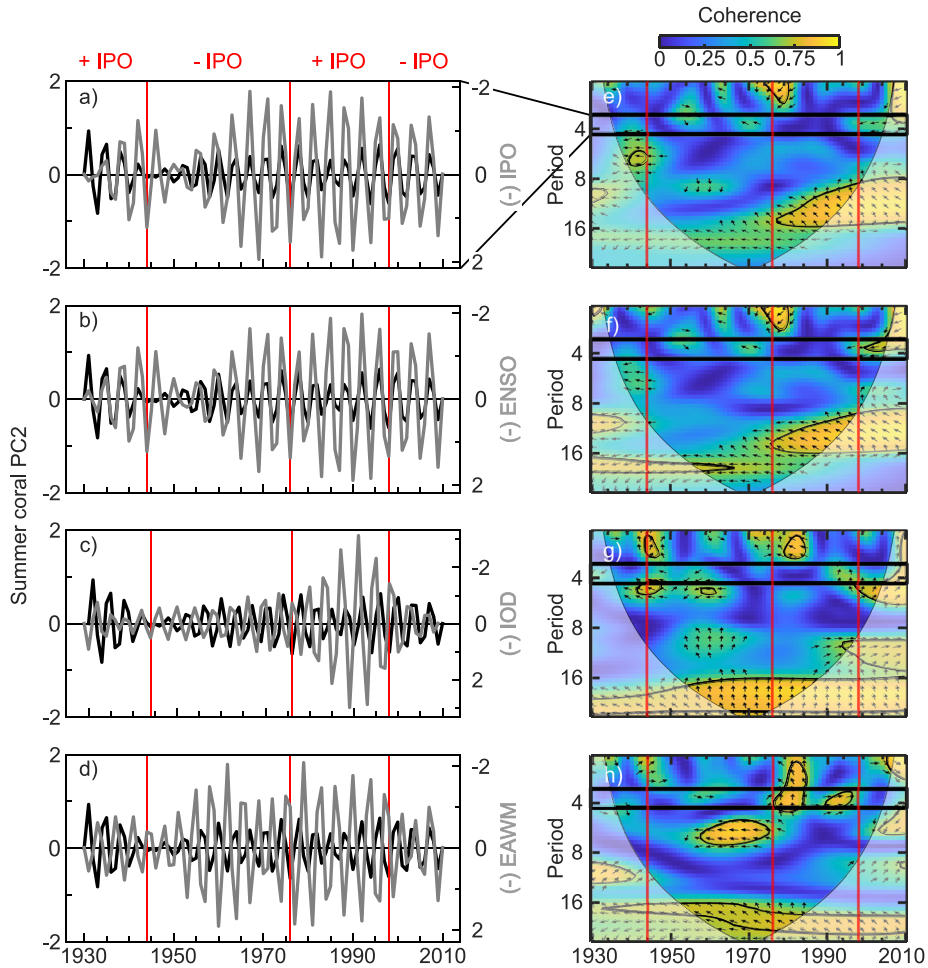

Figure 7. Comparison of summer coral sea surface salinity (SSS) PC2 and climate indices. Band-pass filtered (3.3–4.3 yr) summer PC2 (black solid line) with similarly filtered climate indices (gray solid line) of (a) IPO, (b) ENSO, (c) IOD, and (d) East Asian winter monsoon (EAWM) highlight SSS and climate variability at frequencies describing regional processes. The axes for the climate indices are inverted. Time-varying coherence is examined using wavelet analyses of coral winter PC1 and (e) IPO, (f) ENSO, (g) IOD, and (h) EAWM. The filtered frequencies in panels (a–d) are indicated with black boxes in panels (e–h). Contours (black) in panels (e–h) indicate the 95% confidence level determined against the red noise null hypothesis and arrows describe relative phase relationships. The cone of influence is shown in a lighter shade. For both methods of comparison, the important phase shifts of the IPO in 1944, 1976, and 1998 (England et al., 2014) and the 1976 Indo-Pacific climatic shift are marked with red vertical lines.

filtered IPO and ENSO indices are in phase with the interannual summer PC1 for the entire range of the record (Figures 7a and 7b) while the EAWM index negatively covaries with the record after 1955 (Figure 7d).

3.5. Interaction of Climate Drivers Over the Boreal Winter and Summer

For both the boreal winter and summer, a marked change is observed after the 1976 Indo-Pacific climate shift in PC1, the leading mode of coral reconstructed SSS variability in the MC and SCS. Winter coral PC1 has a consistent interannual (<8 yr per cycle) coherence with the IPO, ENSO, and IOD indices after the shift (Figures 4e–4g). In the summer, a consistent interannual (<8 yr per cycle) and decadal coherence (<16 yr) is only observed between PC1 and ENSO after 1976 (Figure 6f). At lower frequencies (>16 yr), the IOD and EAWM indices retain their influence on both the summer and winter PC1 even after the 1976 climate shift (Figures 4g and 4h, Figures 6g and 6h), while the ENSO and IPO indices shift to higher frequencies (<8 yr for winter PC1 and 8–16 yr for summer PC1; Figures 4e, 4f, 6e, and 6f).

For both seasons, the IPO and ENSO have a similar relationship with PC1 across all frequencies (Figures 4e, 4f, 6e, and 6f). Previous work has recognized the strong similarity between these climate indices suggesting the IPO is a decadal expression of ENSO (Power & Colman, 2006). An alternative interpretation of this observation is that the IPO has a modulating effect on ENSO because it is known to have an asymmetric influence on ENSO's teleconnections. This is observed locally in the records from Palaui with increased advection of saline waters recorded by the site when the PDO and ENSO are in phase (Ramos, Goodkin, Siringan, et al., 2019). Power et al. (1999) found ENSO-induced changes in rainfall over Australia only occur during cold phases of the IPO. Globally, variability in precipitation is dampened when ENSO and IPO are out of phase (Dong et al., 2018). Modulations of the IPO on precipitation and advection of saline Pacific waters into the MC and SCS likely have consequent impacts on regional salinity. Hence, the influence of phases of the IPO on ENSO's relationships with salinity in the SCS and MC are also examined. Over the frequency band 2.5–3.5 yr, ENSO and PC1 are found to be in phase during positive modes of the IPO and vice versa (Figure 4j). Similar modulation of the IOD (Figure 4k) and the EAWM (Figure 4l) by the IPO is not observed suggesting other factors or additional modulation by ENSO might complicate this relationship.

After the 1976 climate shift, ENSO is more consistently coherent with the winter and summer PC1 at timescales of <12 yr per cycle (Figures 4f and 6f). A broader band of frequencies (<8 yr) is observed for the winter suggesting that ENSO impacts propagate through this region across seasons (Wang et al., 2000). An increase in the frequency of ENSO events following the climate shift has been previously observed (Trenberth, 1990) likely resulting from a shift toward negative phases of the Southern Oscillation after 1976 that are associated with weakening easterlies and hence, anomalous warming over the eastern Pacific that is characteristic of El Niño events (Trenberth & Hoar, 1996). Following the 1976 climate shift, the El Niño-like state of the Pacific Ocean reduces the sea level of the eastern equatorial Pacific Ocean and consequently weakens the pressure gradient driving ITF transport (Wainwright et al., 2008). Farther north, a strengthening of the Kuroshio was also observed, leading to an increase in transport through the Luzon Strait into the SCS (Liu et al., 2010). Westward transport into the Luzon Strait is determined by the North Equatorial Current bifurcation latitude that is further affected by ENSO (e.g., Qu et al., 2004). During El Niño, the bifurcation latitude shifts northwards, increasing transport enriched in tropical Pacific waters into the SCS (Gordon et al., 2014, 2012; Qu et al., 2004). ENSO's influence on throughflow transport is known to impact regional salinity through the advection of saline Pacific waters (Gordon et al., 2010). Hence, the increase in ENSO events and the El Niño-like state of the Pacific Ocean after the 1976 climate shift likely has associated impacts on salinity variability that may be captured by PC1. In evaluating SODA SSS before and after the 1976 climate shift (Figure 8), a narrow band of higher salinity is seen from 10°N to 20°N in the equatorial Pacific during the boreal winter and summer (Figures 8c and 8f). If the Pacific Ocean is increasingly in an El Niño state after 1976, there will be a shift northward of the bifurcation latitude that could induce the increased SSS observed from 10°N to 20°N (Figures 8c and 8f).

For both seasons, the IOD has a decadal influence (>16 yr) on PC1 that is significant from 1955 to 1980 (Figures 4g and 6g). The IOD is an interannual climate mode but its decadal modulation has been previously linked to climate variability in the northern and central Pacific Oceans. Annamalai et al. (2005) found that SST anomalies in the Pacific Ocean influence the background state of the eastern Indian Ocean thermocline, defined as the 24°C isothermal depth, by either modulating ITF transport or equatorial winds over the Indian Ocean. Decades when central equatorial Pacific SSTs are persistently warm, and western Pacific SSTs are persistently cool, lead to a shallowing of the thermocline. This enables the upwelling of cooler subsurface waters that precondition the equatorial Indian Ocean for strong positive IOD events. Decadal variation in the Indian Ocean thermocline has also been associated with the IPO. Ocean heat content variability in the Pacific, driven by the IPO, is transmitted to the eastern Indian Ocean through the ITF and also induces shifts in thermocline depth (defined as the 20°C isothermal depth; Jin et al., 2018; Ummenhofer et al., 2020). The IOD is known to feedback to SSS in the MC through its wind-driven modulation of sea level height along the eastern Indian Ocean and hence, the pressure gradient driving the ITF (Sprintall et al., 2009). The positive phase of the IOD lowers sea level height, enhancing ITF transport and consequently altering SSS across the MC. The influence of the IPO on the IOD's signal in both boreal winter and summer coral PC1 (Figures 4c, 4g, 6c, and 6g) is not observed in our analysis, but the strong decadal modulation of SSS variability by the IOD may still be explained by the indirect influence of the IPO or other Pacific decadal variability on thermocline depth in the eastern Indian Ocean.

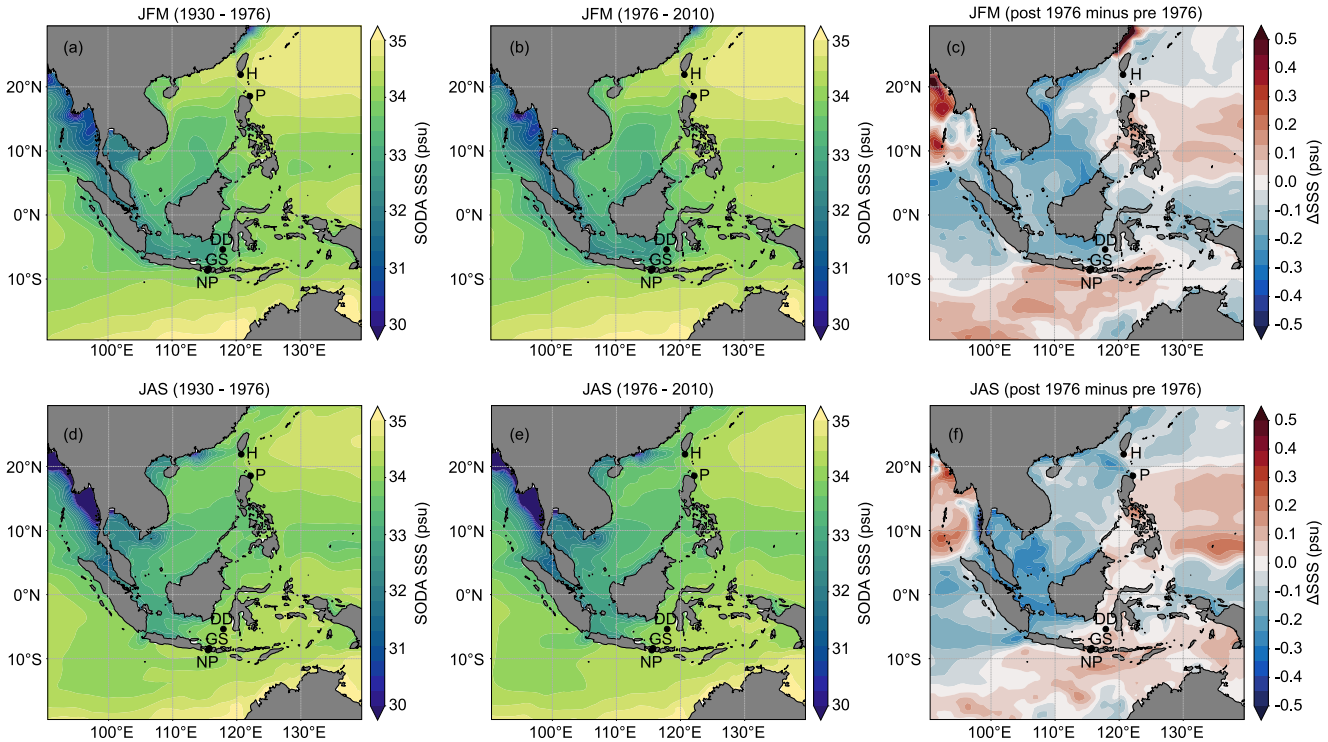

Figure 8. Comparison of regional sea surface salinity (SSS) derived from Simple Ocean Data Assimilation (SODA) v.2.2.4 (Carton & Giese, 2008) before and after the 1976 climate shift. Winter (January–March; JFM) averaged (a) SSS before the 1976 climate shift (1930–1976), (b) SSS after the 1976 climate shift (1976–2010), and (c) SSS before the 1976 climate shift subtracted from SSS after the climate shift. Similarly, summer (July–September; JAS) averaged (e) SSS before the 1976 climate shift (1930–1976), (f) SSS after the 1976 climate shift (1976–2010), and (g) SSS before the 1976 climate shift subtracted from SSS after the climate shift. Coral sites are shown with black dots and labeled as: H = Houbihu, P = Palaui, DD = Doangdoangan Besar, GS = Gili Selang, and NP = Nusa Penida.

In the winter after 1976, the IOD has additional impacts on PC1 at frequencies <12 yr per cycle. The influence of the climate shift on the IOD is nevertheless not well understood. Paleoclimate records indicate that the IOD has been strengthening and becoming more intense since the twentieth century (Abram et al., 2008). After 1960, a trend toward more extreme positive IOD events and a stronger coupling with ENSO has also been observed (Abram et al., 2020). The ENSO and IOD connection to winter PC1 largely occurs over the same interannual bands suggesting a similar potential coupling of these climate systems after the 1976 climate shift that has greater impacts on regional SSS variability (Figures 4f and 4g), as previously suggested (Abram et al., 2020). These SSS impacts may have both oceanic and atmospheric components. Below the surface waters, Kelvin waves generated by anomalous winds and sea level variability during positive IOD events can propagate Indian Ocean impacts farther into the Indonesian Seas (Sprintall et al., 2009), potentially modulating regional salinity. Interactions between ENSO and the IOD also impact precipitation and consequently freshwater input into the MC and SCS, with co-occurring El Niño and positive IOD events weakening monsoon systems across the region (Ummenhofer et al., 2013). Zonal shifts in Walker circulation, which act as an atmospheric bridge between the Indian and the Pacific Ocean, are also driven by ENSO (Hu & Sprintall, 2016) and IOD (Ashok et al., 2003), with a greater divergence of airflow and hence, reduced precipitation over the region during El Niño and positive IOD events. Distinguishing the ENSO and IOD signals in SSS of the outflow regions into the Indian Ocean is challenging (Figure 8). During El Niño events, increased transport of relatively fresh waters from the SCS into the Sulawesi Sea acts as a freshwater plug, blocking flow of Pacific waters into the Makassar Strait through the Mindanao Current (Gordon et al., 2012). Winter monsoonal winds also drive freshened waters from the SCS into the Makassar Strait through the Java Sea (Gordon et al., 2003). Hence, this increased freshening of the Makassar Strait after the 1976, observed in SODA SSS (Figure 8c), may be linked to the increased frequency of El Niño events following the climate shift. In the summer, the monsoonal winds no longer inhibit flow through the Makassar Strait (Gordon et al., 2003). In the summer, the increased SSS of the Makassar Strait (Figure 8f) may be explained by the loss of this freshwater plug. Additionally, the outflow of throughflow waters differs along the Indonesian Seas with relatively freshened waters exiting the region through the Sunda Strait before and after the 1976 climate

shift and for both the winter and summer (Figures 8c and 8f). In contrast, the outflow through the Lombok Strait is more saline across the period examined and for both seasons - matching SSS changes to the Makassar Strait in the summer but not the winter (Figures 8c and 8f). This seasonal variability in SSS in the Lombok Strait may be explained by Ekman transport northward into the Indonesian Seas driven by northeast monsoonal winds in the winter (Susanto et al., 2007). Additional coupling of ENSO, IOD, and the IPO may also enhance the discrepancy in SSS between the Sunda Strait and other straits after the 1976 climate. The response of regional SSS to these coupled climate systems is not well-understood and requires further study.

Like the IOD, the EAWM is coherent with PC1 at frequencies >16 yr per cycle before and after the 1976 climate shift (Figures 4h and 6h). In the winter, the monsoons occur at higher frequencies (<10 yr per cycle) and only over a smaller frequency band (4–7 yr) after 1998 (Figure 4h). This suggests an overall weakening of the EAWM's influence on SSS over the period examined, which is visible in the SODA record by the diminished range of saltier water advected southward into the SCS after 1976 (Figures 8a–8c). The shift in the EAWM is observed locally for coral-based records of winter SSS from Doangdoangan Besar, Gili Selang, and Nusa Penida (Murty et al., 2017, 2018). More regionally, the weakening of winter monsoonal winds in the late twentieth century has been attributed to anthropogenic warming that has reduced the pressure gradient between the Siberian High and Aleutian Low, an important driver of the monsoons (D'Arrigo et al., 2005; Hori & Ueda, 2006; Xu et al., 2006). ENSO teleconnections to the western North Pacific also influence the strength of the EAWM. During El Niño events, the formation of anomalous anticyclonic circulation over the western North Pacific drives southeasterly winds over the SCS and MC that oppose the northwesterly flow of the monsoonal winds and consequently weaken the EAWM (Wang et al., 2000). The PDO describes decadal SST variability in the North Pacific (Mantua et al., 1997; Newman et al., 2016) and has similar impacts on atmospheric circulation during its positive phase. Hence, a positive PDO and ENSO acting in phase can further weaken the EAWM (Kim et al., 2014). Monsoon winds are an important driver of seasonal surface transport and associated SSS variability in the ITF and SCSTF (Gordon et al., 2003; Qu et al., 2000). With their weakening influence, other drivers of transport like ENSO and the IOD that have occurred more frequently in recent years may play a more dominant role in the region. This could also explain ENSO and IOD's strong signal in boreal winter and summer PC1 after the 1976 climate shift.

While not independently significant, both seasonal PC2s document the contribution of Nusa Penida on SSS variability. The limited wavelet coherence of seasonal PC2s with corresponding regional SODA PC2s observed using cross-coherence analysis (Figures 3b and 3d) suggests that this mode describes the impacts of climate variability specifically on the Lombok Strait. In the winter, PC2 is coherent with the EAWM at frequencies <16 yr per cycle both before and after the 1976 climate shift (Figure 5h). At higher frequencies, ENSO and IOD are also coherent with PC2 during negative modes of the IPO (Figures 5f and 5g). In the summer, a trend similar to winter PC1 is observed. ENSO shifts to consistently high-frequency (8–16 yr) SSS impacts after the 1976 climate shift (Figure 7f), while the IOD and EAWM have a lower frequency signal (>16 yr) in PC2 throughout the record (Figures 7g and 7h). In the Lombok Strait, northwestern winds associated with the winter monsoon drive northward flow of Indian Ocean waters into the Strait through Ekman pumping that inhibit southward transport of ITF waters (Susanto et al., 2007). The Lombok Strait flow reverses in the boreal summer. SSS variability described by winter PC2 therefore may be more closely associated with the monsoons, while summer SSS variability may be impacted by the modulation of waters advected into the Lombok Strait driven by the IOD and ENSO.

4. Conclusions

EOF analysis of coral records across the SCS and MC are used to examine the climate drivers of regional SSS. For both the boreal winter and summer, the 1976 Indo-Pacific climate shift emerges as a time of change to the dominant influences on SSS variability in two principal ways.

1. At low frequencies (>8 yr per cycle), the IOD and the EAWM retain their influence on both winter and summer salinity throughout the study period (1930–2010). ENSO impacts on SSS shift entirely to higher frequencies after the 1976 climate shift.
   The IOD and EAWM generally occur at interannual timescales. Decadal variation of the IOD has been attributed to oceanic teleconnections of the IPO (Jin et al., 2018; Ummenhofer et al., 2020) while decadal trends in the EAWM are related to atmospheric teleconnections of the more localized PDO (Kim et al., 2014). ENSO is also modulated by these low-frequency climate systems (Dong et al., 2018; Power et al., 1999), but its recent

intensification and increased variability has been directly linked to the 1976 climate shift (Trenberth, 1990). Based on our analysis, this broader low-frequency behavior of the IOD, the EAWM, and ENSO has associated influences on SSS variability in the SCS and MC. Why the IOD and the EAWM do not display shifts in low-frequency SSS impacts as a result of the 1976 Indo-Pacific climate shift, for example, ENSO, requires further study.

2. At higher frequencies (<8 yr per cycle), ENSO and the IOD become critical drivers of winter salinity after the 1976 climate shift while the EAWM influence weakens.

   The intensification and strengthening of the ENSO and IOD in recent decades has been previously observed (Abram et al., 2020; Trenberth, 1990), coincident with a weakening of the EAWM (D'Arrigo et al., 2005; Hori & Ueda, 2006; Xu et al., 2006). Only the shift to an El Niño-like state of the Pacific Ocean has been directly linked to the 1976 Indo-Pacific climate shift (Trenberth, 1990). The impact of the shift on the IOD and the EAWM requires further study, but the overlapping high-frequency signal of ENSO and IOD in winter SSS variability after 1976 suggests that their interaction through their influence on circulation in the ITF (Hameed, 2018; Sprintall et al., 2009) may have a more dominant impact on regional salinity than in previous decades.

The shift to external drivers of SSS variability that originate in the Indian and Pacific Ocean, particularly the IOD and ENSO, as a result of the 1976 Indo-Pacific climate shift indicates broader changes to throughflow transport in the SCS and MC. This may also have implications for global thermohaline circulation through the return of modified Pacific Ocean surface waters to the Atlantic Ocean (Gordon, 1986).

Data Availability Statement

Coral δ^{18}O data from Palaui (P, https://www.ncdc.noaa.gov/paleo/study/27271), Houbihu (H, https://www.ncdc.noaa.gov/paleo/study/29412), Doangdoangan Besar (DD, https://www.ncdc.noaa.gov/paleo/study/24630), Gili Selang (GS, https://www.ncdc.noaa.gov/paleo/study/25290), and Nusa Penida (NP, https://www.ncdc.noaa.gov/paleo/study/25290) is publicly available on the NOAA NCEI Paleoclimatology database. SODAv2.2.4, the salinity reanalysis product examined, is also publicly available and can be accessed through APDRC (http://apdrc.soest.hawaii.edu/datadoc/soda_2.2.4.php). EOF analysis is performed using the principal component analysis functionalities of the Python scikit -learn library (https://scikit-learn.org/stable/modules/generated/sklearn.decomposition.PCA.html). Filter design utilizes the signal processing module of the Python SciPy library (https://docs.scipy.org/doc/scipy/reference/signal.html?highlight=signal#module-scipy.signal). Code for cross-coherence analysis using a multitaper method with adaptive weighting and bias correction can be accessed at https://www.mathworks.com/matlabcentral/fileexchange/22551-multi-tapercoherencemethod-with-bias-correction. Code for wavelet coherence analysis can be accessed at http://grinsted.github.io/wavelet-coherence/.

Acknowledgments
The authors would like to thank Dr. C. Gnanaseelan and two anonymous reviewers for their insightful and thoughtful comments that significantly improved the original manuscript. The authors are also grateful for the help of D. Wu, M. Dominguez, N. Baigorria, S. Chan, and S. Martinez (from the Brown Scholars Program at the American Museum of Natural History) in analysis of the coral records. This research is supported by the Helen Gurley Brown Foundation and the American Museum of Natural History through the Helen Fellowship Post-Baccalaureate Residency. This work was also supported by the US National Science Foundation under AGS-2101214 (J. E. Smerdon) and AGS—2002083 (S. A. Murty). D. Samanta was partially supported by the Singapore Ministry of Education Academic Research Fund MOE2019-T3-1-004. This is Earth Observatory of Singapore contribution number 447.

References

Abram, N. J., Dixon, B. C., Rosevear, M. G., Plunkett, B., Gagan, M. K., Hantoro, W. S., & Phipps, S. J. (2015). Optimized coral reconstructions of the Indian Ocean Dipole: An assessment of location and length considerations. *Paleoceanography*, *30*(10), 1391–1405. https://doi.org/10.1002/2015PA002810

Abram, N. J., Gagan, M. K., Cole, J. E., Hantoro, W. S., & Mudelsee, M. (2008). Recent intensification of tropical climate variability in the Indian Ocean. *Nature Geoscience*, *1*(12), 849–853. https://doi.org/10.1038/ngeo357

Abram, N. J., Wright, N. M., Ellis, B., Dixon, B. C., Wurtzel, J. B., England, M. H., et al. (2020). Coupling of Indo-Pacific climate variability over the last millennium. *Nature*, *579*(7799), 385–392. https://doi.org/10.1038/s41586-020-2084-4

Annamalai, H., Potemra, J., Murtugudde, R., & McCreary, J. P. (2005). Effect of preconditioning on the extreme climate events in the tropical Indian Ocean. *Journal of Climate*, *18*(17), 3450–3469. https://doi.org/10.1175/JCLI3494.1

Ashok, K., Guan, Z., & Yamagata, T. (2003). Influence of the Indian Ocean Dipole on the Australian winter rainfall. *Geophysical Research Letters*, *30*(15). https://doi.org/10.1029/2003GL017926

Basnett, T. A., & Parker, D. E. (1997). Development of the Global Mean Sea Level Pressure Data Set GMSLP2 (Technical Note No. CRTN79). *Hadley Center for Climate Prediction and Research*. http://cedadocs.ceda.ac.uk/1080/1/Development_of_the_Global_Mean_Sea_Level_Pressure_Data_Set_GMSLP2.pdf

Bjerknes, J. (1969). Atmospheric teleconnections from the equatorial Pacific. *Monthly Weather Review*, *97*(3), 163–172. https://doi.org/10.1175/1520-0493(1969)097<0163:ATFTEP>2.3.CO;2

Cahyarini, S. Y., Pfeiffer, M., Nurhati, I. S., Aldrian, E., Dullo, W.-C., & Hetzinger, S. (2014). Twentieth century sea surface temperature and salinity variations at Timor inferred from paired coral δ^{18}O and Sr/Ca measurements. *Journal of Geophysical Research: Oceans*, *119*(7), 4593–4604. https://doi.org/10.1002/2013JC009594

Carton, J. A., Chepurin, G., & Cao, X. (2000). A Simple Ocean Data Assimilation analysis of the global upper ocean 1950–95. Part II: Results. *Journal of Physical Oceanography*, *30*(2), 311–326. https://doi.org/10.1175/1520-0485(2000)030<0311:ASODAA>2.0.CO;2

Carton, J. A., & Giese, B. S. (2008). A reanalysis of ocean climate using Simple Ocean Data Assimilation (SODA). *Monthly Weather Review*, *136*(8), 2999–3017. https://doi.org/10.1175/2007MWR1978.1

Caruso, M. J., Gawarkiewicz, G. G., & Beardsley, R. C. (2006). Interannual variability of the Kuroshio intrusion in the South China Sea. *Journal of Oceanography*, *62*(4), 559–575. https://doi.org/10.1007/s10872-006-0076-0

Centurioni, L. R., Niiler, P. P., & Lee, D.-K. (2004). Observations of inflow of Philippine Sea Surface water into the South China Sea through the Luzon Strait. *Journal of Physical Oceanography*, *34*, 9. https://doi.org/10.1175/1520-0485(2004)034<0113:ooiops>2.0.co;2

Chakravorty, S., Chowdary, J. S., & Gnanaseelan, C. (2014). Epochal changes in the seasonal evolution of tropical Indian Ocean warming associated with El Niño. *Climate Dynamics*, *42*(3–4), 805–822. https://doi.org/10.1007/s00382-013-1666-3

Charles, C. D., Cobb, K., Moore, M. D., & Fairbanks, R. G. (2003). Monsoon-tropical ocean interaction in a network of coral records spanning the 20th century. *Marine Geology*, *201*(1–3), 207–222. https://doi.org/10.1016/S0025-3227(03)00217-2

D'Arrigo, R., Wilson, R., Panagiotopoulos, F., & Wu, B. (2005). On the long-term interannual variability of the East Asian winter monsoon. *Geophysical Research Letters*, *32*(21), L21706. https://doi.org/10.1029/2005GL023235

Dong, B., Dai, A., Vuille, M., & Timm, O. E. (2018). Asymmetric modulation of ENSO teleconnections by the interdecadal Pacific oscillation. *Journal of Climate*, *31*(18), 7337–7361. https://doi.org/10.1175/JCLI-D-17-0663.1

Du, Y., & Qu, T. (2010). Three inflow pathways of the Indonesian throughflow as seen from the Simple Ocean Data Assimilation. *Dynamics of Atmospheres and Oceans*, *50*(2), 233–256. https://doi.org/10.1016/j.dynatmoce.2010.04.001

Dunbar, R. B., & Wellington, G. M. (1981). Stable isotopes in a branching coral monitor seasonal temperature variation. *Nature*, *293*(5832), 453–455. https://doi.org/10.1038/293453a0

England, M. H., & Huang, F. (2005). On the interannual variability of the Indonesian throughflow and its linkage with ENSO. *Journal of Climate*, *18*(9), 1435–1444. https://doi.org/10.1175/JCLI3322.1

England, M. H., McGregor, S., Spence, P., Meehl, G. A., Timmermann, A., Cai, W., et al. (2014). Recent intensification of wind-driven circulation in the Pacific and the ongoing warming hiatus. *Nature Climate Change*, *4*(3), 222–227. https://doi.org/10.1038/nclimate2106

Epstein, S., Buchsbaum, R., Lowenstam, H. A., & Urey, H. C. (1953). Revised carbonate-water isotopic temperature scale. *The Geological Society of America Bulletin*, *64*(11), 1315. https://doi.org/10.1130/0016-7606(1953)64[1315:RCITS]2.0.CO;2

Fang, G., Susanto, R. D., Soesilo, I., Zheng, Q., Qiao, F., & Wei, Z. (2005). A note on the South China Sea shallow interocean circulation. *Advances in Atmospheric Sciences*, *22*(6), 946–954. https://doi.org/10.1007/BF02918693

Giese, B. S., & Ray, S. (2011). El Niño variability in Simple Ocean Data Assimilation (SODA), 1871–2008. *Journal of Geophysical Research*, *116*(C2), C02024. https://doi.org/10.1029/2010JC006695

Godfrey, J. S. (1996). The effect of the Indonesian throughflow on ocean circulation and heat exchange with the atmosphere: A review. *Journal of Geophysical Research*, *101*(C5), 12217–12237. https://doi.org/10.1029/95JC03860

Good, S. A., Martin, M. J., & Rayner, N. A. (2013). EN4: Quality controlled ocean temperature and salinity profiles and monthly objective analyses with uncertainty estimates. *Journal of Geophysical Research: Oceans*, *118*(12), 6704–6716. https://doi.org/10.1002/2013JC009067

Gordon, A. L. (1986). Interocean exchange of thermocline water. *Journal of Geophysical Research*, *91*(C4), 5037–5046. https://doi.org/10.1029/JC091iC04p05037

Gordon, A. L. (2001). Interocean exchange. In G. Siedler, J. Church, & J. Gould (Eds.), *Ocean circulation and climate* (Vol. 77, pp. 303–314). Academic Press. https://doi.org/10.1016/S0074-6142(01)80125-X

Gordon, A. L., Flament, P., Villanoy, C., & Centurioni, L. (2014). The nascent Kuroshio of Lamon Bay. *Journal of Geophysical Research: Oceans*, *119*(7), 4251–4263. https://doi.org/10.1002/2014JC009882

Gordon, A. L., Huber, B. A., Metzger, E. J., Susanto, R. D., Hurlburt, H. E., & Adi, T. R. (2012). South China Sea throughflow impact on the Indonesian throughflow: Makassar Strait throughflow profile. *Geophysical Research Letters*, *39*(11). https://doi.org/10.1029/2012GL052021

Gordon, A. L., Sprintall, J., Van Aken, H. M., Susanto, D., Wijffels, S., Molcard, R., et al. (2010). The Indonesian throughflow during 2004–2006 as observed by the INSTANT program. *Dynamics of Atmospheres and Oceans*, *50*(2), 115–128. https://doi.org/10.1016/j.dynatmoce.2009.12.002

Gordon, A. L., Susanto, R. D., & Vranes, K. (2003). Cool Indonesian throughflow as a consequence of restricted surface layer flow. *Nature*, *425*(6960), 824–828. https://doi.org/10.1038/nature02038

Graham, N. (1994). Decadal-scale climate variability in the tropical and North Pacific during the 1970s and 1980s: Observations and model results. *Climate Dynamics*, *10*, 135–162. https://doi.org/10.1007/BF00210626

Grinsted, A., Moore, J. C., & Jevrejeva, S. (2004). Application of the cross wavelet transform and wavelet coherence to geophysical time series. *Nonlinear Processes in Geophysics*, *11*(5/6), 561–566. https://doi.org/10.5194/npg-11-561-2004

Grottoli, A. G., & Eakin, C. M. (2007). A review of modern coral $\delta^{18}O$ and $\Delta^{14}C$ proxy records. *Earth-Science Reviews*, *81*(1–2), 67–91. https://doi.org/10.1016/j.earscirev.2006.10.001

Hameed, S. N. (2018). *The Indian Ocean Dipole* (Vol. 1). Oxford University Press. https://doi.org/10.1093/acrefore/9780190228620.013.619

Henley, B. J., Gergis, J., Karoly, D. J., Power, S., Kennedy, J., & Folland, C. K. (2015). A tripole index for the Interdecadal Pacific Oscillation. *Climate Dynamics*, *45*(11–12), 3077–3090. https://doi.org/10.1007/s00382-015-2525-1

Hori, M. E., & Ueda, H. (2006). Impact of global warming on the East Asian winter monsoon as revealed by nine coupled atmosphere-ocean GCMs. *Geophysical Research Letters*, *33*(3), L03713. https://doi.org/10.1029/2005GL024961

Hu, S., & Sprintall, J. (2016). Interannual variability of the Indonesian throughflow: The salinity effect. *Journal of Geophysical Research: Oceans*, *121*(4), 2596–2615. https://doi.org/10.1002/2015JC011495

Huybers, P., & Denton, G. (2008). Antarctic temperature at orbital timescales controlled by local summer duration. *Nature Geoscience*, *1*(11), 787–792. https://doi.org/10.1038/ngeo311

Ishii, M., & Kimoto, M. (2009). Reevaluation of historical ocean heat content variations with time-varying XBT and MBT depth bias corrections. *Journal of Oceanography*, *65*(3), 287–299. https://doi.org/10.1007/s10872-009-0027-7

Jin, X., Kwon, Y.-O., Ummenhofer, C. C., Seo, H., Schwarzkopf, F. U., Biastoch, A., et al. (2018). Influences of Pacific climate variability on decadal subsurface ocean heat content variations in the Indian Ocean. *Journal of Climate*, *31*(10), 4157–4174. https://doi.org/10.1175/JCLI-D-17-0654.1

Kim, J.-W., Yeh, S.-W., & Chang, E.-C. (2014). Combined effect of El Niño-Southern Oscillation and Pacific decadal oscillation on the East Asian winter monsoon. *Climate Dynamics*, *42*(3–4), 957–971. https://doi.org/10.1007/s00382-013-1730-z

Krawczyk, H., Zinke, J., Browne, N., Struck, U., McIlwain, J., O'Leary, M., & Garbe-Schönberg, D. (2020). Corals reveal ENSO-driven synchrony of climate impacts on both terrestrial and marine ecosystems in northern Borneo. *Scientific Reports*, *10*(1), 3678. https://doi.org/10.1038/s41598-020-60525-1

Lau, K.-M., & Li, M.-T. (1984). The monsoon of East Asia and its global associations—A survey. *Bulletin of the American Meteorological Society*, *65*(2), 114–125. https://doi.org/10.1175/1520-0477(1984)065<0114:TMOEAA>2.0.CO;2

Liang, W.-D., Yang, Y. J., Tang, T. Y., & Chuang, W.-S. (2008). Kuroshio in the Luzon Strait. *Journal of Geophysical Research*, *113*(C8), C08048. https://doi.org/10.1029/2007JC004609

Linsley, B. K., Wu, H. C., Rixen, T., Charles, C. D., Gordon, A. L., & Moore, M. D. (2017). SPCZ zonal events and downstream influence on surface ocean conditions in the Indonesian throughflow region. *Geophysical Research Letters*, *44*(1), 293–303. https://doi.org/10.1002/2016GL070985

Liu, Q., Wang, D., Zhou, W., Xie, Q., & Zhang, Y. (2010). Covariation of the Indonesian throughflow and South China Sea throughflow associated with the 1976/1977 regime shift. *Advances in Atmospheric Sciences*, *27*(1), 87–94. https://doi.org/10.1007/s00376-009-8061-3

Mantua, N. J., Hare, S. R., Zhang, Y., Wallace, J. M., & Francis, R. C. (1997). A Pacific interdecadal climate oscillation with impacts on salmon production. *Bulletin of the American Meteorological Society*, *78*(6), 1069–1079. https://doi.org/10.1175/1520-0477(1997)078<1069:APICOW>2.0.CO;2

Masumoto, Y., & Yamagata, T. (1996). Seasonal variations of the Indonesian throughflow in a general ocean circulation model. *Journal of Geophysical Research*, *101*(C5), 12287–12293. https://doi.org/10.1029/95JC03870

McCulloch, M. T., Gagan, M. K., Mortimer, G. E., Chivas, A. R., & Isdale, P. J. (1994). A high-resolution Sr/Ca and δ^{18}O coral record from the Great Barrier Reef, Australia, and the 1982–1983 El Niño. *Geochimica et Cosmochimica Acta*, *58*(12), 2747–2754. https://doi.org/10.1016/0016-7037(94)90142-2

Meehl, G. A., Hu, A., & Santer, B. D. (2009). The mid-1970s climate shift in the Pacific and the relative roles of forced vs. inherent decadal variability. *Journal of Climate*, *22*(3), 780–792. https://doi.org/10.1175/2008JCLI2552.1

Meyers, G., Bailey, R. J., & Worby, A. P. (1995). Geostrophic transport of Indonesian throughflow. *Deep Sea Research Part I: Oceanographic Research Papers*, *42*(7), 1163–1174. https://doi.org/10.1016/0967-0637(95)00037-7

Murtugudde, R., & Busalacchi, A. J. (1998). Salinity effects in a tropical ocean model. *Journal of Geophysical Research*, *103*(C2), 3283–3300. https://doi.org/10.1029/97JC02438

Murty, S. A., Goodkin, N. F., Halide, H., Natawidjaja, D., Suwargadi, B., Suprihanto, I., et al. (2017). Climatic influences on southern Makassar Strait salinity over the past century: Climate influence on Makassar Strait SSS. *Geophysical Research Letters*, *44*(23), 11967–11975. https://doi.org/10.1002/2017GL075504

Murty, S. A., Goodkin, N. F., Wiguna, A. A., & Gordon, A. L. (2018). Variability in coral-reconstructed sea surface salinity between the northern and southern Lombok Strait linked to East Asian winter monsoon mean state reversals. *Paleoceanography and Paleoclimatology*, *33*(10), 1116–1133. https://doi.org/10.1029/2018PA003387

Nan, F., Xue, H., & Yu, F. (2015). Kuroshio intrusion into the South China Sea: A review. *Progress in Oceanography*, *137*, 314–333. https://doi.org/10.1016/j.pocean.2014.05.012

Nan, F., Yu, F., Xue, H., Zeng, L., Wang, D., Yang, S., & Nguyen, K.-C. (2016). Freshening of the upper ocean in the South China Sea since the early 1990s. *Deep Sea Research Part I: Oceanographic Research Papers*, *118*, 20–29. https://doi.org/10.1016/j.dsr.2016.10.010

Newman, M., Alexander, M. A., Ault, T. R., Cobb, K. M., Deser, C., Di Lorenzo, E., et al. (2016). The Pacific decadal oscillation, revisited. *Journal of Climate*, *29*(12), 4399–4427. https://doi.org/10.1175/JCLI-D-15-0508.1

Overland, J. E., & Preisendorfer, R. W. (1981). A significance test for principal components applied to a cyclone climatology. *Monthly Weather Review*, *110*(1), 1–4. https://doi.org/10.1175/1520-0493(1982)110<0001:ASTFPC>2.0.CO;2

Power, S., Casey, T., Folland, C., Colman, A., & Mehta, V. (1999). Inter-decadal modulation of the impact of ENSO on Australia. *Climate Dynamics*, *15*(5), 319–324. https://doi.org/10.1007/s003820050284

Power, S., & Colman, R. (2006). Multiyear predictability in a coupled general circulation model. *Climate Dynamics*, *26*(2–3), 247–272. https://doi.org/10.1007/s00382-005-0055-y

Qu, T., Kim, Y. Y., Yaremchuk, M., Tozuka, T., Ishida, A., & Yamagata, T. (2004). Can Luzon Strait transport play a role in conveying the impact of ENSO to the South China Sea? *Journal of Climate*, *17*, 14. https://doi.org/10.1175/1520-0442(2004)017<3644:CLSTPA>2.0.CO;2

Qu, T., Mitsudera, H., & Yamagata, T. (2000). Intrusion of the North Pacific waters into the South China Sea. *Journal of Geophysical Research: Oceans*, *105*(C3), 6415–6424. https://doi.org/10.1029/1999JC900323

Qu, T., Song, Y. T., & Yamagata, T. (2009). An introduction to the South China Sea throughflow: Its dynamics, variability, and application for climate. *Dynamics of Atmospheres and Oceans*, *47*(1–3), 3–14. https://doi.org/10.1016/j.dynatmoce.2008.05.001

Ramos, R. D., Goodkin, N. F., Druffel, E. R. M., Fan, T. Y., & Siringan, F. P. (2019). Interannual coral Δ^{14}C records of surface water exchange across the Luzon Strait. *Journal of Geophysical Research: Oceans*, *124*(1), 491–505. https://doi.org/10.1029/2018JC014735

Ramos, R. D., Goodkin, N. F., & Fan, T.-Y. (2020). Coral records at the northern edge of the western Pacific warm pool reveal multiple drivers of sea surface temperature, salinity, and rainfall variability since the end of the Little Ice Age. *Paleoceanography and Paleoclimatology*, *35*(5), e2019PA003826. https://doi.org/10.1029/2019PA003826

Ramos, R. D., Goodkin, N. F., Siringan, F. P., & Hughen, K. A. (2017). *Diploastrea heliopora* Sr/Ca and δ^{18}O records from northeast Luzon, Philippines: An assessment of interspecies coral proxy calibrations and climate controls of sea surface temperature and salinity. *Paleoceanography*, *32*(4), 424–438. https://doi.org/10.1002/2017PA003098

Ramos, R. D., Goodkin, N. F., Siringan, F. P., & Hughen, K. A. (2019). Coral records of temperature and salinity in the tropical western Pacific reveal influence of the Pacific decadal oscillation since the late nineteenth century. *Paleoceanography and Paleoclimatology*, *34*(8), 1344–1358. https://doi.org/10.1029/2019PA003684

Rayner, N. A., Horton, E. B., Parker, D. E., Folland, C. K., & Hackett, R. B. (1996). Version 2.2 of the Global Sea-Ice and Sea Surface Temperature Dataset, 1903–1994 (Technical Note No. CRTN74). Hadley Center for Climate Prediction and Research. https://www.metoffice.gov.uk/hadobs/gisst/crtn74.pdf

Rayner, N. A., Parker, D. E., Horton, E. B., Folland, C. K., Alexander, L. V., Rowell, D. P., et al. (2003). Global analyses of sea surface temperature, sea ice, and night marine air temperature since the late nineteenth century. *Journal of Geophysical Research*, *108*(D14), 4407. https://doi.org/10.1029/2002JD002670

Saji, N. H., Goswami, B. N., Vinayachandran, P. N., & Yamagata, T. (1999). A dipole mode in the tropical Indian Ocean. *Nature*, *401*(6751), 360–363. https://doi.org/10.1038/43854

Samanta, D., Goodkin, N. F., & Karnauskas, K. B. (2021). Volume and heat transport in the South China Sea and Maritime Continent at present and the end of the 21st century. *Journal of Geophysical Research: Oceans*, *126*(9), e2020JC016901. https://doi.org/10.1029/2020JC016901

Sarachik, E. S., & Cane, M. A. (2010). *The El Niño-Southern Oscillation phenomenon*. Cambridge University Press. https://doi.org/10.1017/CBO9780511817496

Schoenefeldt, R., & Schott, F. A. (2006). Decadal variability of the Indian Ocean cross-equatorial exchange in SODA. *Geophysical Research Letters*, *33*(8), L08602. https://doi.org/10.1029/2006GL025891

Sprintall, J., Gordon, A. L., Koch-Larrouy, A., Lee, T., Potemra, J. T., Pujiana, K., & Wijffels, S. E. (2014). The Indonesian seas and their role in the coupled ocean-climate system. *Nature Geoscience*, *7*(7), 487–492. https://doi.org/10.1038/ngeo2188

Sprintall, J., Wijffels, S., Gordon, A. L., Ffield, A., Molcard, R., Susanto, R. D., et al. (2004). INSTANT: A new international array to measure the Indonesian throughflow. *Eos, Transactions American Geophysical Union*, *85*(39), 369. https://doi.org/10.1029/2004EO390002

Sprintall, J., Wijffels, S. E., Molcard, R., & Jaya, I. (2009). Direct estimates of the Indonesian throughflow entering the Indian Ocean: 2004–2006. *Journal of Geophysical Research*, *114*(C7), C07001. https://doi.org/10.1029/2008JC005257

Susanto, R. D., & Gordon, A. L. (2005). Velocity and transport of the Makassar Strait throughflow. *Journal of Geophysical Research*, *110*(C1), C01005. https://doi.org/10.1029/2004JC002425

Susanto, R. D., Gordon, A. L., & Sprintall, J. (2007). Observations and proxies of the surface layer throughflow in Lombok Strait. *Journal of Geophysical Research*, *112*(C3), C03S92. https://doi.org/10.1029/2006JC003790

Thomson, R. E., & Emery, W. J. (2014). Chapter 4—The spatial analyses of data fields. In R. E. Thomson, & W. J. Emery (Eds.), *Data analysis methods in physical oceanography*, 3rd ed., (pp. 313–424). Elsevier. https://doi.org/10.1016/B978-0-12-387782-6.00004-1

Tillinger, D., & Gordon, A. L. (2009). Fifty years of the Indonesian throughflow. *Journal of Climate*, *22*(23), 6342–6355. https://doi.org/10.1175/2009JCLI2981.1

Titchner, H. A., & Rayner, N. A. (2014). The Met Office Hadley Centre sea ce and sea surface temperature data set, version 2: 1. Sea ice concentrations. *Journal of Geophysical Research: Atmospheres*, *119*(6), 2864–2889. https://doi.org/10.1002/2013JD020316

Trenberth, K. E. (1990). Recent observed interdecadal climate changes in the Northern Hemisphere. *Bulletin of the American Meteorological Society*, *71*(7), 988–993. https://doi.org/10.1175/1520-0477(1990)071<0988:ROICCI>2.0.CO;2

Trenberth, K. E. (1997). The definition of El Nino. *Bulletin of the American Meteorological Society*, *78*(12), 8. https://doi.org/10.1175/1520-0477(1997)078<2771:tdoeno>2.0.co;2

Trenberth, K. E., & Hoar, T. J. (1996). The 1990–1995 El Niño-Southern Oscillation event: Longest on record. *Geophysical Research Letters*, *23*(1), 57–60. https://doi.org/10.1029/95GL03602

Ummenhofer, C. C., D'Arrigo, R. D., Anchukaitis, K. J., Buckley, B. M., & Cook, E. R. (2013). Links between Indo-Pacific climate variability and drought in the Monsoon Asia Drought Atlas. *Climate Dynamics*, *40*(5–6), 1319–1334. https://doi.org/10.1007/s00382-012-1458-1

Ummenhofer, C. C., Ryan, S., England, M. H., Scheinert, M., Wagner, P., Biastoch, A., & Böning, C. W. (2020). Late 20th century Indian Ocean heat content gain masked by wind forcing. *Geophysical Research Letters*, *47*(22), e2020GL088692. https://doi.org/10.1029/2020GL088692

Wainwright, L., Meyers, G., Wijffels, S., & Pigot, L. (2008). Change in the Indonesian throughflow with the climatic shift of 1976/1977. *Geophysical Research Letters*, *35*(3), L03604. https://doi.org/10.1029/2007GL031911

Wang, B., Luo, X., Yang, Y.-M., Sun, W., Cane, M. A., Cai, W., et al. (2019). Historical change of El Niño properties sheds light on future changes of extreme El Niño. *Proceedings of the National Academy of Sciences*, *116*(45), 22512–22517. https://doi.org/10.1073/pnas.1911130116

Wang, B., Wu, R., & Fu, X. (2000). Pacific–East Asian teleconnection: How does ENSO affect East Asian climate? *Journal of Climate*, *13*(9), 1517–1536. https://doi.org/10.1175/1520-0442(2000)013<1517:PEATHD>2.0.CO;2

Wu, B., & Wang, J. (2002). Winter Arctic oscillation, Siberian high and East Asian winter monsoon. *Geophysical Research Letters*, *29*(19), 3-1–3-4. https://doi.org/10.1029/2002GL015373

Wu, R., & Kirtman, B. P. (2004). Understanding the impacts of the Indian Ocean on ENSO variability in a coupled GCM. *Journal of Climate*, *17*(20), 4019–4031. https://doi.org/10.1175/1520-0442(2004)017<4019:UTIOTI>2.0.CO;2

Wyrtki, K. (1961). Physical Oceanography of the Southeast Asian waters. Naga Report, 2.

Wyrtki, K. (1987). Indonesian throughflow and the associated pressure gradient. *Journal of Geophysical Research*, *92*(C12), 12941–12946. https://doi.org/10.1029/JC092iC12p12941

Xu, M., Chang, C.-P., Fu, C., Qi, Y., Robock, A., Robinson, D., & Zhang, H. (2006). Steady decline of East Asian monsoon winds, 1969–2000: Evidence from direct ground measurements of wind speed. *Journal of Geophysical Research*, *111*(D24), D24111. https://doi.org/10.1029/2006JD007337

Zhang, Z., & Moore, J. C. (2015). Empirical orthogonal functions. In *Mathematical and physical fundamentals of climate change* (pp. 161–197). Elsevier. https://doi.org/10.1016/B978-0-12-800066-3.00006-1